AMERICAN JOURNAL OF PHYSIOLOGY
HEART AND CIRCULATORY PHYSIOLOGY

Am J Physiol Heart Circ Physiol 322: H549–H567, 2022.
First published January 28, 2022; doi:10.1152/ajpheart.00460.2021

RESEARCH ARTICLE

Vascular Biology and Microcirculation

Electronic cigarette exposure causes vascular endothelial dysfunction due to NADPH oxidase activation and eNOS uncoupling

Mohamed A. El-Mahdy,[1]* Mohamed G. Ewees,[1]* Mahmoud S. Eid,[1] Elsayed M. Mahgoup,[1] Sahar A. Khaleel,[1,2] and Jay L. Zweier[1]

[1]*Center for Environmental and Smoking Induced Disease and the Division of Cardiovascular Medicine, Department of Internal Medicine, Davis Heart & Lung Research Institute, College of Medicine, The Ohio State University, Columbus, Ohio and*
[2]*Department of Pharmacology and Toxicology, College of Pharmacy, Al-Azhar University, Cairo, Egypt*

Abstract

We recently reported a mouse model of chronic electronic cigarette (e-cig) exposure-induced cardiovascular pathology, where long-term exposure to e-cig vape (ECV) induces cardiac abnormalities, impairment of endothelial function, and systemic hypertension. Here, we delineate the underlying mechanisms of ECV-induced vascular endothelial dysfunction (VED), a central trigger of cardiovascular disease. C57/BL6 male mice were exposed to ECV generated from e-cig liquid containing 0, 6, or 24 mg/mL nicotine for 16 and 60 wk. Time-dependent elevation in blood pressure and systemic vascular resistance were observed, along with an impairment of acetylcholine-induced aortic relaxation in ECV-exposed mice, compared with air-exposed control. Decreased intravascular nitric oxide (NO) levels and increased superoxide generation with elevated 3-nitrotyrosine levels in the aorta of ECV-exposed mice were observed, indicating that ECV-induced superoxide reacts with NO to generate cytotoxic peroxynitrite. Exposure increased NADPH oxidase expression, supporting its role in ECV-induced superoxide generation. Downregulation of endothelial nitric oxide synthase (eNOS) expression and Akt-dependent eNOS phosphorylation occurred in the aorta of ECV-exposed mice, indicating that exposure inhibited de novo NO synthesis. Following ECV exposure, the critical NOS cofactor tetrahydrobiopterin was decreased, with a concomitant loss of its salvage enzyme, dihydrofolate reductase. NADPH oxidase and NOS inhibitors abrogated ECV-induced superoxide generation in the aorta of ECV-exposed mice. Together, our data demonstrate that ECV exposure activates NADPH oxidase and uncouples eNOS, causing a vicious cycle of superoxide generation and vascular oxidant stress that triggers VED and hypertension with predisposition to other cardiovascular disease.

NEW & NOTEWORTHY Underlying mechanisms of e-cig-induced vascular endothelial dysfunction are delineated. e-cig exposure activates and increases expression of NADPH oxidase and disrupts activation and coupling of eNOS, leading to a vicious cycle of superoxide generation and peroxynitrite formation, with tetrahydrobiopterin depletion, causing loss of NO that triggers vascular endothelial dysfunction. This process is progressive, increasing with the duration of e-cig exposure, and is more severe in the presence of nicotine, but observed even with nicotine-free vaping.

e-cigarettes; eNOS uncoupling; NADPH oxidase; tetrahydrobiopterin; vascular endothelial dysfunction

INTRODUCTION

The endothelium is a dynamic organ lining the entire circulatory system, from the heart to the smallest capillaries. Endothelial cells maintain vascular homeostasis and are involved in a myriad of vascular functions, including modulation of vascular tone, maintenance of blood fluidity, and regulation of inflammation and angiogenesis (1). Endothelial vasodilator function is mediated by endothelium-derived relaxing factor, identified as the gaseous molecule nitric oxide (NO) (2). NO is synthesized in the endothelium by endothelial NO synthase (eNOS), which catalyzes the conversion of L-arginine and molecular oxygen to NO and L-citrulline (3). This process requires the cofactor tetrahydrobiopterin (BH_4) and the electron donor NADPH (4). Once synthesized, NO diffuses across the endothelial cell into the adjacent smooth muscle cells, where it triggers vasodilation through activation of soluble guanylate cyclase and opposes the actions of endothelium-derived contracting factors such as angiotensin II and endothelin-1 (5–7).

* M. A. El-Mahdy and M. G. Ewees contributed equally to this work.
Correspondence: J. L. Zweier (jay.zweier@osumc.edu).
Submitted 19 August 2021 / Revised 4 January 2022 / Accepted 24 January 2022

Vascular endothelial dysfunction (VED) predisposes to various cardiovascular diseases (8). Impaired endothelium-dependent relaxation is typically caused by alterations in the NO-mediated smooth muscle relaxation cascade pathway (9). Oxidative stress, with the elevated production of reactive oxygen species (ROS), is a well-known trigger of VED (10). Superoxide rapidly scavenges NO to form the toxic oxidant peroxynitrite (11, 12). Furthermore, ROS degrades the redox-sensitive NOS cofactor BH_4, resulting in eNOS uncoupling, in which the enzyme switches from the synthesis of NO to superoxide (13, 14). Among the major sources of ROS in the vasculature, uncoupled eNOS and NADPH oxidases are of particular importance (15, 16). Uncoupled eNOS produces superoxide instead of NO due to disruption in its NO synthase function (17, 18). The NOX family of NADPH oxidases consists of seven transmembrane enzymes, the NOX complexes that transport electrons across biological membranes to reduce molecular oxygen to superoxide. NOX2, also known as gp^{91phox}, is the prototype NADPH oxidase (19). Several studies revealed the contribution of NOX2 to vascular remodeling and dysfunction through the induction of vascular oxidative stress (20–22).

Humans are increasingly exposed to a wide variety of ROS-generating toxins and chemicals, including those from tobacco smoking and the recently developed electronic cigarettes (e-cig). Since their development, e-cig have been claimed as a safer alternative to tobacco cigarettes (TC), and this has led to a rapid increase in their use (23). However, vaping-related illnesses have been reported, and toxic chemicals, similar to those found in TC smoke, have been detected in e-cig aerosol, raising concerns over the health risk posed by e-cig use (24). E-cig have been identified as a source of oxidative stress in experimental animals and in humans (25). Although tobacco smoking is well-established as a major risk factor for cardiovascular disease (26, 27), this has not been well-studied with e-cig, and data on chronic effects of e-cig use are limited (28, 29). We recently developed a mouse model of chronic vaping-induced cardiovascular dysfunction and hypertension (30), and we and others have reported that long-term e-cig vape (ECV) exposure induces cardiac abnormalities, impairment of endothelial function, and systemic hypertension (HTN) (30–33). However, questions remain regarding the underlying mechanisms by which this occurs.

In the current work, we utilized our recently reported long-term mouse model of chronic e-cig vaping (30), which mimics chronic human use, to delineate the mechanisms involved in e-cig exposure-induced VED. We investigated the role of NADPH oxidase and eNOS uncoupling in ROS generation, the main trigger of VED, in the vasculature of ECV-exposed mice. The current study demonstrates that ECV exposure activates NADPH oxidase and disrupts the activation and coupling of eNOS, causing a vicious cycle of superoxide generation and NOS uncoupling that led to VED. This work provides insights on the underlying molecular mechanisms by which long-term e-cig exposure causes VED and cardiovascular disease.

MATERIALS AND METHODS

Materials

Chemicals, reagents, and other materials were obtained from Millipore Sigma (St. Louis, MO) unless noted otherwise.

Animals and e-Cig Exposure Protocol

This study was reviewed and approved by the Institutional Laboratory Animal Care and Use Committee (IACUC) of The Ohio State University and conformed to the National Institutes of Health Guidelines for the Care and Use of Laboratory Animals.

Sixteen-week-old male C57BL/6J mice were purchased from the Jackson Laboratory (Bar Harbor, ME), acclimatized for 2 wk, and randomly divided into four groups: air-exposed control group and three ECV-exposed groups with different nicotine (NIC) concentrations. ECV-exposed mice were exposed 5 days per week for 16 or 60 wk to e-cig aerosol generated from e-cig liquid (Apollo, Future Technology, Inc.) containing NIC 0 mg/mL (ECV-0), 6 mg/mL (ECV-6), or 24 mg/mL (ECV-24). Exposure was performed as previously described (30), using a computer-controlled high-throughput vaping exposure system built in our laboratory as previously described (34). Briefly, mice were exposed to 20 cycles each cycle consisting of ~3.2 min of e-cig aerosol, followed by 2 min of fresh air purge and 5 s of rest. In our custom-built exposure system, we used a commercially available e-cig box-device (JoyeTech, eVic Basic) with Tobeco Super Tank MINI 4 mL capacity and 0.2 Ω coil made of Kanthal (iron/chromium/aluminum wire). The e-cig atomizer power was set at 25 W, with 2.24 V and 5 s firing.

Vascular Reactivity Assessment

Preparation of the isolated mouse aorta was similar to that previously described (35). Briefly, the thoracic aorta was gently dissected from anesthetized and heparinized mice and cut transversely into rings of 2–3 mm length. These rings were mounted on a wire Myograph (Multi Myograph System-610M, Danish Myo, Hinnerup, Denmark) with care taken to avoid endothelial damage, suspended in 5-mL baths containing modified Krebs-Henseleit buffer (KHB) (in mM): 118 NaCl, 24 $NaHCO_3$, 4.6 KCl, 1.2 NaH_2PO_4, 1.2 $CaCl_2$, 4.6 HEPES, and 18 glucose, pH 7.4, at 37°C and continuously purged with 95% O_2-5% CO_2. Rings were equilibrated for 90 min with an initial resting tension of 1 g, and the bathing solution was then changed at 15-min intervals. Changes in isometric tension were recorded on a PowerLab/8sp data-acquisition system (AD Instruments, Colorado Springs, CO) using ADI Chart software (version 5.3). After equilibration, the responsiveness, stability, and maximal constriction of each ring were first tested with 50 mM KCl. The responsiveness of each ring was then measured by the successive dose escalating administration of L-phenylephrine hydrochloride (phenylephrine, PE) up to 1 μM concentration (30). The integrity of the vascular endothelium was then assessed pharmacologically by acetylcholine (ACh)-induced relaxation of the phenylephrine-pre-contracted rings. Dose-response relaxation to cumulative concentrations of ACh (10 nM, 100 nM, 1 μM, 10 μM, and 100 μM) was recorded through changes in isometric tension. After the ACh measurements and washing the rings three times, similar measurements were also performed measuring the relaxation with sodium nitroprusside (SNP) (1 nM, 10 nM, 100 nM, 1 μM, and 10 μM) to assess the endothelial-independent vasodilatory response. The concentration of agonist in the organ bath was increased in steps of 1-log units.

ACh or SNP was added to yield the next higher concentration when the response to the lower dose reached a steady level. The vasodilator (relaxant) responses were expressed as percent decreases of PE-induced pre-contraction, where the contraction produced by PE in each ring from its initial resting tension was considered as 100%. In preliminary control experiments, with administration of the eNOS inhibitor N^G-nitro-L-arginine methyl ester (L-NAME, 1 mM), ACh-induced relaxation was inhibited by >90%, consistent with prior studies of mouse aortic rings (6). The dose-response curves were graphed by connecting line fit with line passing through all data points. ACh and SNP concentrations that induced 50% relaxation (RC_{50}) were calculated from fitted ACh/SNP-relaxation response curves using TableCurve 2 D, version 5.01, purchased from SYSTAT Software Inc. (Palo Alto, CA).

Blood Pressure Measurement

Blood pressure (BP) was measured by the noninvasive tail-cuff method, in lightly sedated mice, using a CODA high-throughput BP acquisition system (Kent Scientific Inc., Torrington, CT). Briefly, mice were trained for 7 days by measuring BP daily before collecting actual data. Mice were initially anesthetized using 2.0% isoflurane in O_2 at a rate of 0.8 L/min, and anesthesia was maintained with 1% isoflurane. Mice were then placed on a warming platform and allowed to acclimatize for 10 min before readings were obtained. BP recordings were made twice. Each BP measurement session consisted of five acclimatization cycles followed by 15 BP measurements cycles. On the data collection day, two sessions of 15 BP measurements were obtained, and the average of accepted readings from both sessions was used for systolic BP (SBP), diastolic BP (DBP), and mean arterial BP (MABP) in each individual mouse (36). The computer software of the CODA system measures the systolic and diastolic pressures with inflation of a pneumatic tail cuff while a transducer measures the BP waveform. The software determines signal-to-noise and accepted readings, discarding noisy inaccurate measurements.

Echocardiography

Transthoracic echocardiography was performed using a VisualSonics Vevo 2100 high-frequency, high-resolution ultrasound system (Visual Sonics, Toronto, Canada) to measure in vivo left ventricular (LV) function, as reported previously (6). Mice were initially anesthetized using 2.0% isoflurane in 95% O_2, 5% CO_2 at a rate of 0.8 L/min, and anesthesia was maintained with 1% isoflurane. ECG sensors and a rectal temperature probe were attached, and the mouse was placed supine on the heated platform. Body temperature, heart rate (HR), and respiratory rate were continuously monitored. The ultrasonic probe was then placed on the left thorax and ultrasound beam directed to the mid papillary muscle level to obtain M-mode and B-mode echocardiography images in the parasternal long- and short-axis views. As reported in our prior publication (30), LV end-diastolic volume and LV end-systolic volume were measured to calculate stroke volume (SV), and along with the measured heart rate (HR), the cardiac output (CO) was calculated as SV × HR (37). Systemic vascular resistance (SVR) was calculated using the equation SVR = mean arterial blood pressure (MABP)/CO (37).

In Situ Detection of Superoxide in the Aorta

Dihydroethidium (DHE)-derived fluorescence was used to determine superoxide generation in the aorta. The aorta was cleaned from adipose and connective tissue, cut into 3-mm rings, and placed in optimal cutting temperature (OCT; Tissue-Tek, Sakura Finetek, Inc., Torrance, CA) embedding compound. Frozen OCT blocks were cut at 5-μm sections using a cryotome (Leica Biosystem CM3050S, Vista, CA). Sections were collected on super-frosted slides and stained in the dark with DHE (10 μM) (Molecular Probes, Inc., Eugene, OR) either alone or together with NADPH oxidase inhibitors GSK2795039 (GSK; 100 μM) and 3-benzyl-7-(2-benzoxazolyl)thio-1,2,3-triazolo[4,5-d]pyrimidine (VAS2870; VAS, 10 μM) or NOS inhibitor N^G-nitro-L-arginine methyl ester (L-NAME; 1 mM). Sections were washed with phosphate-buffered saline (PBS), anti-fade mounting medium (Southern Biotechnology Associates, Birmingham, AL) containing the nuclear stain 4′,6-diamidino-2-phenylindole dihydrochloride (DAPI; 1 μM) was applied, and a coverslip was placed. ROS-generated fluorescence authenticity was confirmed by quenching the DHE signal with 100 μM of the superoxide dismutase mimetic (SODm) Mn (III) tetrakis (4-benzoic acid) porphyrin chloride (MnTBAP). At least five fields per section were captured at ×40 using a confocal microscope (FluoView 3000; Olympus America Inc., Center Valley, PA), and fluorescence intensity was analyzed using the FluoView 3000 provided software in at least four sections per animal with six mice per group. DHE-derived fluorescence was detected at excitation wavelength 490 nm and emission wavelength 555 nm.

In Situ Detection of Nitric Oxide in the Aorta

Indirect NO measurements were performed using a cell-permeable fluorescent probe 4-amino-5-methylamino-2',7'-difluorescein diacetate (DAF-FM; Chemodex LTD, St. Gallen, Switzerland) as described earlier (38), with minor modifications. Briefly, the aorta was isolated, cleaned, and maintained in KHB containing 1 μM ACh for 15 min, cut into ~ 3-mm rings, placed in OCT embedding compound, and cut to 5-μm sections on super-frosted slides, using a Leica BiosystemCM3050S cryostat. Sections were incubated with 8 μM DAF-FM at 37°C for 30 min in the dark and washed with PBS. Anti-fade mounting medium containing 1 μM of the nuclear stain DAPI was applied, and a coverslip was placed. To test the authenticity and the source of NO-generated fluorescence, some slides were incubated with 100 μM of NO trap 2-(4-carboxyphenyle)-4,4,5,5-tetramethylimidazoline-1-oxyl-3-oxide (C-PTIO; Dojindo Molecular Technologies, Inc., Rockville, MD) for 15 min at 37°C, before DAF-FM. At least five fields were captured at ×40 using a FluoView 3000 confocal microscope. Fluorescence intensity was analyzed using the microscope-provided software in at least four sections per animal, four animals per group. DAF-FM-derived fluorescence was detected at λex 495 nm, λem 515 nm.

Western Blot Analysis

Whole cell protein extracts were obtained after homogenization of the aorta in lysis buffer containing 62 mM Tris (pH 6.8), 10% glycerol, and 2% sodium dodecyl sulfate. Samples were heated at 70°C for 5 min and cooled down, and then, protein concentration was determined using the Bio-Rad DC

protein assay kit (Bio-Rad, Hercules, CA). Proteins were loaded (40 μg protein/sample) and separated in a graded (4–20%) polyacrylamide gel (Bio-Rad, Hercules, CA) and electroblotted on PVDF membranes (Bio-Rad, Hercules, CA). Membranes were blocked with 5% nonfat dry milk in Tris-buffered saline-tween 20 (TBST) for 1°h at 37°C and washed three times with TBST. The following primary rabbit polyclonal antibodies were purchased from Invitrogen, Waltham, MA, and used according to the manufacturer's recommended concentration: anti-eNOS (1:500 dilution), anti-p-eNOS ser^{1177} (1:500 dilution), anti-dihydrofolate reductase enzyme (DHFR; 1:1,000 dilution), and anti-nitrotyrosine (1:1,000 dilution). Rabbit polyclonal anti-NOX2 (1:1,000 dilution) was purchased from Proteintech, IL. Rabbit polyclonal anti-p-Akt Ser473 (1:1,000 dilution), anti-GAPDH (1:2000 dilution), and anti-rabbit linked to horseradish peroxidase (HRP) secondary antibodies (1:2,000 dilution) were purchased from Cell Signaling Technology, Danvers, MA. Membranes were incubated with primary antibodies overnight at 4°C then washed in TBST and incubated with secondary antibodies for 1 h at 37°C. Membranes were then developed using the Western blotting detection reagent (Clarity Max Western ECL, Hercules, CA). Protein bands were captured and analyzed using a high-resolution KwikQuant Imager and KwikQuantImage Manager Software, respectively (Kindle Biosciences LLC., Greenwich, CT). The bands were normalized to GAPDH band intensity.

Immunofluorescence Staining

The aorta was isolated, cleaned, placed in OCT embedding compound, and kept at −80°C until further processing. Frozen OCT blocks were cryosectioned in 5 μm and placed on chilled super-frosted slides. Sections were washed with PBS containing 0.5% tween (PBST), permeabilized using 0.5% Triton-X, and fixed using 2% paraformaldehyde for 10 min. Sections were blocked for nonspecific binding by 10% goat serum and 1% bovine serum albumin in PBST and incubated overnight with primary antibodies at 4°C. Slides were washed three times with PBST and incubated with a fluorescent secondary antibody (Invitrogen, Waltham, MA) for 30 min at room temperature. Anti-fade mounting medium containing 1 μM of the nuclear stain DAPI was applied, and a coverslip was placed. The following antibodies were used: rabbit polyclonal anti-eNOS (1:100 dilution, Invitrogen, Waltham, MA), rabbit monoclonal anti-p-eNOS Ser^{1177} (1:100 dilution, Cell Signaling, Danvers, MA), mouse monoclonal anti-nitrotyrosine (1:50 dilution, Santa Cruz Biotechnology Inc., Dallas, TX), and mouse monoclonal anti-NOX2, (1:50 dilution, Santa Cruz Biotechnology Inc., Dallas, TX). Sections were then incubated with a secondary antibody for 1 h. The following secondary antibodies were purchased from Invitrogen and used at 1:1,000 dilution: anti-rabbit and anti-mouse Alexa Fluor 594 and Alexa Fluor 488. Sections were digitally imaged by confocal microscopy, different fields were captured, and the fluorescence intensity was quantitated and normalized to DAPI using ImageJ in at least four sections per animal, with at least four fields visualized per section, and six animals per group.

Tetrahydrobiopterin Measurement

Tetrahydrobiopterin (BH_4) in aortic tissue homogenate was measured using a colorimetric ELISA kit (MyBioSource, San Diego, CA) that applies the competitive immunoassay technique utilizing a mouse polyclonal anti-BH_4 antibody, an BH_4-HRP conjugate, and a substrate for HRP enzyme. The product of the enzyme-substrate reaction forms a blue-colored complex that will turn yellow after adding a reaction stop solution. The intensity of yellow color is measured spectrophotometrically at 450 nm in a microplate reader.

The experiment was done according to the manufacturer's instructions. Briefly, the aorta was cleaned, rinsed with PBS, and homogenized in ice-cold PBS using a glass homogenizer. Aortic homogenates were ultrasonicated by pulsing three times for 10 s, each separated by at least 30 s, with the sample tube kept on ice, and then centrifuged for 15 min at 1,500 *g* to separate clean supernatants. Then, 100 μL of samples or standards was added into ELISA plate wells followed by 10 μL of balance solution (provided with the kit) and 50 μL of BH_4-HRP conjugate. The plate was mixed well and incubated for 1 h at 37°C. Wells were washed using a wash solution (provided with the kit), 50 μL of each substrate was added to each well, and the plate was incubated for 20 min at 37°C. The reaction was terminated, and the absorbance was measured at a wavelength of 450 nm using SpectraMax plus microplate reader (Molecular Devices, CA). A standard curve was plotted and used to quantitate BH_4 in samples. Concentrations were normalized to total protein content in each sample.

Statistical Analysis

Most data were analyzed by two-way ANOVA with Bonferroni post hoc analysis, considering exposure groups and exposure time. Where there was only one exposure time, one-way ANOVA with Bonferroni post hoc analysis was performed comparing the treatment groups at the one exposure time. For the vascular relaxation data curves, repeated-measures two-way ANOVA was used. These statistical tests and analyses were performed using GraphPad InStat software, version 3.06 (GraphPad, San Diego, CA). Data are presented as means ± SE. Statistical differences were considered significant if $P \leq 0.05$.

RESULTS

ECV Exposure Triggers Vascular Endothelial Dysfunction

To verify the presence of exposure-dependent VED, we assessed the effect of ECV exposure on ACh-induced endothelium-dependent and SNP-induced endothelium-independent vascular relaxation (Fig. 1, *A*–*D*). ACh and SNP concentrations that induced 50% relaxation (RC_{50}) on a PE-preconstricted aortic rings were calculated from fitted ACh/SNP-relaxation response curves as described in the METHODS section (Table 1).

After 16 wk of exposure, ECV-0-, ECV-6-, and ECV-24-exposed aorta exhibited a reduction in endothelium-dependent relaxation, as evidenced by the rightward and upward shift in the ACh concentration-dependent relaxation curve compared with that of air-exposed aorta. RC_{50} was increased from 42 ± 5 nM in the air-exposed group to 156 ± 13 nM, 270 ± 18 nM, and 650 ± 25 nM, respectively, in the ECV-0, ECV-6, and ECV-24 groups (all $P < 0.04$). Although the maximal relaxation, R_{max}, in air-exposed aortas was 95 ± 4% of the

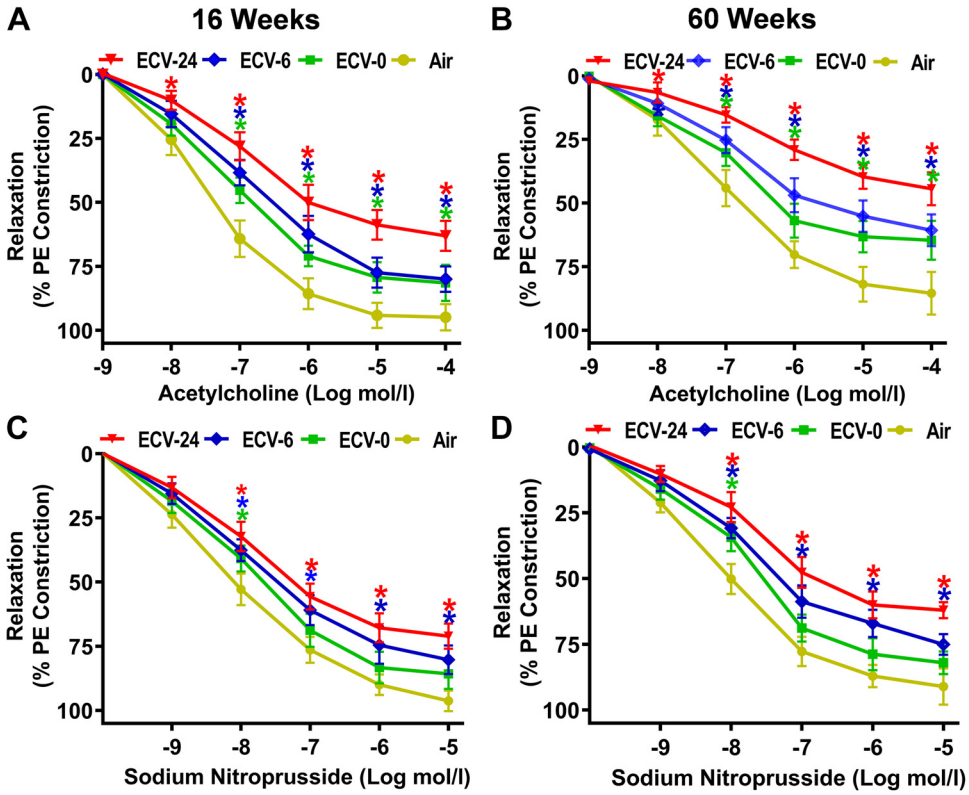

Figure 1. Endothelium-dependent and -independent vascular relaxation. Male C57BL/6J mice were exposed to 16 or 60 wk of either air or electronic cigarette (e-cig) vape generated from e-cig liquid containing nicotine (NIC) 0 mg/mL (ECV-0), 6 mg/mL (ECV-6), or 24 mg/mL (ECV-24). For endothelium-dependent function, aortic rings from 16-wk-exposed (*A*) and 60-wk-exposed (*B*) mice were mounted in a wire myograph, constricted by 1 μM phenylephrine (PE), and acetylcholine response curve was derived. For endothelium-independent function, aortic rings from 16-wk-exposed (*C*) and 60-wk-exposed (*D*) mice were constricted by 1 μM PE, and sodium nitroprusside response curve was derived. Data are presented as means ± SE of 6 mice. Analysis was done using repeated-measures two-way ANOVA. The differences were considered statistically significant at $P \leq 0.05$. *Significant difference from relative air-exposed controls.

PE-induced constriction, ECV-0-, ECV-6-, and ECV-24-exposed aortas exhibited significantly lower R_{max} values of 82 ± 3%, 79 ± 5%, and 64 ± 4% relaxation, respectively (all $P <$ 0.05) (Fig. 1*A*; Table 1). With 60 wk of ECV exposure, even larger reductions in endothelium-dependent relaxation were seen. RC_{50} was increased in ECV-0 and ECV-6 to 745 ± 21 nM (P = 0.037) and 1,390 ± 41 nM (P = 0.001), respectively, compared with 154 ± 6 nM in the air-exposed group. In ECV-24-exposed aortic rings, 50% relaxation did not occur. ECV-0-, ECV-6-, and ECV-24-exposed aortas exhibited 65 ± 4, 60 ± 6, and 44 ± 4% of maximal relaxation, respectively, all significantly lower ($P <$ 0.01), compared with 85 ± 4 relaxation in air-exposed aortas (Fig. 1*B*; Table 1). These exposure duration-dependent changes were consistent with those previously reported (30). Full intergroup statistical analysis was done to compare means among all groups and to verify the statistical differences between 16- and 60-wk exposures for each group as presented in Table 1.

Table 1. *Endothelium-dependent and -independent vascular reactivity data*

	RC_{50}, nM		R_{max}, %	
	16 wk	60 wk	16 wk	60 wk
Acetylcholine				
Air	42 ± 5	154 ± 6	95 ± 4	85 ± 4
ECV-0	156 ± 13*	745 ± 21*$	82 ± 3*	65 ± 4*$
ECV-6	270 ± 18*#	1,390 ± 41*#$	79 ± 5*	60 ± 6*$
ECV-24	650 ± 25*#@	–	64 ± 4*#@	44 ± 4*#@$
Sodium nitroprusside				
Air	8.0 ± 0.7	8.6 ± 2	96 ± 5	94 ± 7
ECV-0	19 ± 2*	22 ± 3*	85 ± 6	80 ± 4*$
ECV-6	34 ± 4*#	54 ± 4*#$	80 ± 2*	75 ± 4*
ECV-24	54 ± 4*#@	92 ± 5*#@$	68 ± 3*#@	58 ± 3*#@$

Values are means ± SE. ECV-0, electronic cigarette (e-cig) vape generated from e-cig liquid containing nicotine 0 mg/mL; ECV-6, electronic cigarette (e-cig) vape generated from e-cig liquid containing nicotine 6 mg/mL; ECV-24, electronic cigarette (e-cig) vape generated from e-cig liquid containing nicotine 24 mg/mL; RC_{50}, concentration of acetylcholine/sodium nitroprusside that produces 50% relaxation of phenylephrine-preconstricted aortic rings; R_{max}, maximum acetylcholine/sodium nitroprusside-induced relaxation. *$P <$ 0.05, significant from air-exposed controls; #$P <$ 0.05, significant from ECV-0; @$P <$ 0.05, significant from ECV-6; $$P <$ 0.05, significant from the same exposure at 16 wk.

Vessels from ECV-exposed mice also exhibited significant alterations in endothelium-independent relaxation compared with those from air-exposed mice at both 16 and 60 wk of exposure (Fig. 1, *C* and *D*, Table 1). However, these alterations are not as large as those seen for endothelium-dependent relaxation. After 16 wk of exposure, shifts in RC_{50} of SNP from 8 ± 0.7 nM in the air-exposed controls to 19 ± 2 (P = 0.05), 34 ± 4 (P = 0.048), and 54 ± 4 (P = 0.029) nM in the ECV-0, ECV-6, and ECV-24 groups, respectively, were seen (Table 1). Maximum relaxation values also decreased from 96 ± 5% in air control to 85 ± 6 (P = 0.058), 80 ± 2 (P = 0.05), and 68 ± 3% (P = 0.04) in the ECV-0, ECV-6, and ECV-24 groups, respectively. After 60 wk of exposure, further shifts in the RC_{50} values (nM) from 8.6 ± 2 in the air-exposed controls to 22 ± 3, 54 ± 4, and 92 ± 5 in the ECV-0, ECV-6, and ECV-24 groups, respectively, (all $P <$ 0.05) were seen. Maximum relaxation values also decreased from 94 ± 7% in air control to 80 ± 4 (P = 0.05), 75 ± 4 (P = 0.048), and 58 ± 3% (P = 0.039) in the ECV-0, ECV-6, and ECV-24 groups, respectively (Table 1). Thus, similar to endothelium-dependent relaxation, the endothelium-independent relaxation is also

impaired with ECV exposures; however, the magnitude of this dysfunction is less. Full intergroup and exposure time comparisons are presented in Table 1.

ECV Exposure Increases Blood Pressure and Systemic Vascular Resistance

As VED predisposes to hypertension and other cardiovascular disease (39), we further measured BP and systemic vascular resistance (SVR) following ECV exposure. Initial measurements of BP were performed at baseline before and after 16 and 60 wk of exposure to verify the onset and severity of vascular disease. Baseline values of systolic blood pressure (SBP) and diastolic blood pressure (DBP) were 104 ± 4 mmHg and 72 ± 3 mmHg, respectively (Fig. 2, *A* and *B*). The baseline mean arterial blood pressure (MABP) was 83 ± 3 mmHg (Fig. 2*C*). At 16 wk of exposure, ECV-6 and ECV-24 groups exhibited significant elevations in BP compared with the air-exposed group, with SBP of 123 ± 6 mmHg (P = 0.049) and 133 ± 8 mmHg (P = 0.0007), respectively, (Fig. 2*A*); DBP of 86 ± 6 mmHg (P = 0.05) and 93 ± 4 mmHg ($P < 0.0007$), respectively, (Fig. 2*B*); and MABP of 98 ± 5 mmHg (P = 0.049) and 106 ± 7 mmHg (P = 0.0007), respectively. Although the ECV-0 group showed higher BP values than the air-exposed group, these values did not reach statistical significance at 16 wk of exposure (Fig. 2*C*). With extended exposure duration to 60 wk, further progressive elevations in BP were observed in the ECV-0, ECV-6, and ECV- 24 groups. Marked elevation of BP was seen in ECV-24 mice, compared with air-exposed controls, with SBP, DBP, and MABP values of 158 ± 8, 110 ± 5, and 126 ± 8 mmHg, respectively, (all $P < 0.0001$). In ECV-6 mice, although elevated BP was present, BP values tended to be less than that in ECV-24 mice, with SBP of 141 ± 7, DBP of 99 ± 4, and MABP of 112 ± 5, all $P < 0.0002$, compared with values in the air-exposed group. Furthermore, at 60 wk of exposure, the elevations in SBP, DBP, and MABP were significant in ECV-0 mice with values of 142 ± 4, 98 ± 6, and 113 ± 7 mmHg, respectively, all $P < 0.0001$, when compared with the air-exposed group. In contrast to this, for the air-exposed mice, BP did not significantly change over time with values of 104 ± 8 and 109 ± 4 mmHg for SBP, 72 ± 7 and 76 ± 5 mmHg for DBP, and 83 ± 6 and 87 ± 3 mmHg for MABP, at *weeks 16* and *60* of exposure, respectively. More complete statistical analysis between the groups and exposure times was done as presented in Fig. 2, *A–C*.

We calculated SVR using the equation SVR = MABP/cardiac output (CO). CO was measured by echocardiography as reported previously (37), calculated from the product of left ventricular stroke volume and heart rate. As in the prior study (30), the heart rate values were similar in the four groups studied at either time point with mean values ranging from 467 to 481 at 16 wk of exposure and from 478 to 511 at 60 wk of exposure. CO was lower in all ECV groups compared with air-exposed controls (data not shown). In the air-exposed group, SVR was calculated as 345 ± 18 and 343 ± 19 dyn/s/cm^{-5} at 16 and 60 wk of exposure, respectively (Fig. 2*D*). In the ECV-0 group, only a slight increase in SVR to 369 ± 20 (P = 0.069) dyn/s/cm^{-5} was seen at 16 wk of exposure; however, after 60 wk of exposure, SVR was clearly increased to 533 ± 15 dyn/s/cm^{-5} (P = 0.037). At 16 wk of exposure, both the ECV-6 and ECV-24 groups exhibited a significant elevation in SVR, reaching 424 ± 15 (P = 0.047) and 529 ± 13 (P = 0.036) dyn/s/cm^{-5}, respectively. Higher SVR values of 554 ± 17 (P = 0.036) and 624 ± 19 dyn/s/cm^{-5} (P = 0.025) were reported following 60 wk of exposure to the ECV-6 and ECV-24 groups, respectively (Fig. 2*D*). More complete statistical analysis between the groups and exposure times was done as presented in Fig. 2*D*. Thus, consistent with our prior study (30), e-cig exposure resulted in a NIC and exposure time-dependent VED with elevated blood pressure and SVR. However, questions remain regarding the molecular mechanisms by which ECV induces VED.

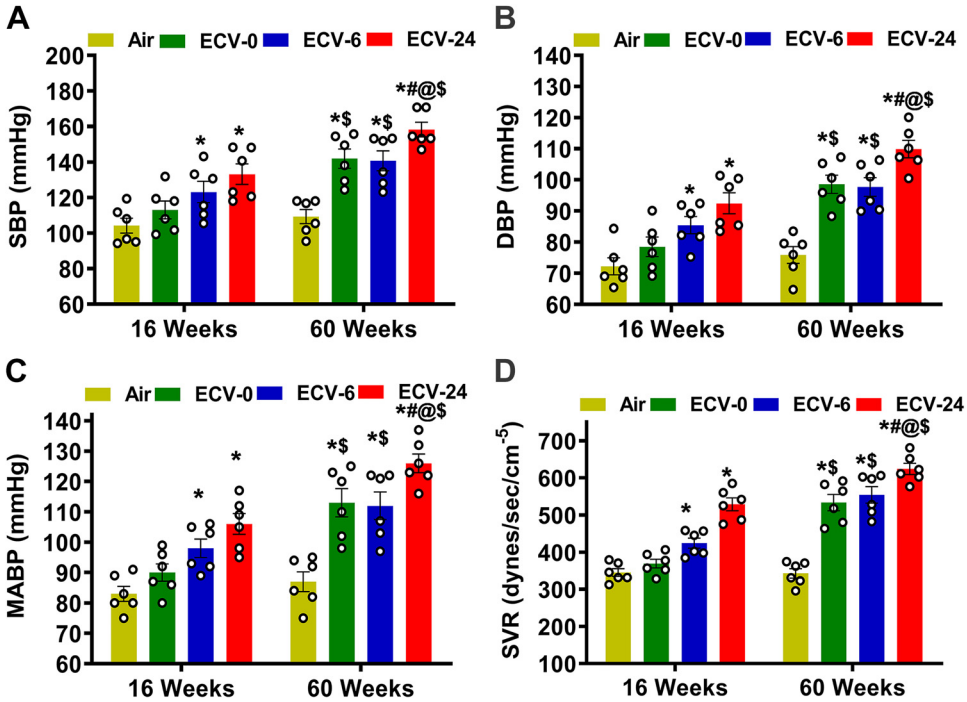

Figure 2. Blood pressure and vascular resistance. Male C57BL/6J mice were exposed to 16 or 60 wk of either air or electronic cigarette (e-cig) vape generated from e-cig liquid containing nicotine (NIC) 0 mg/mL (ECV-0), 6 mg/mL (ECV-6), or 24 mg/mL (ECV-24). *A*: systolic blood pressure (SBP). *B*: diastolic blood pressure (DBP). *C*: mean arterial blood pressure (MABP). *D*: systemic vascular resistance (SVR). ECV exposure resulted in a NIC- and an exposure time-dependent vascular endothelial dysfunction with elevated MABP and SVR. Data are presented as means ± SE of 6 mice. Each point represents the average of at least 10 measurements per animal. Analysis was done using two-way ANOVA followed by Bonferroni multiple-comparisons test. The differences were considered statistically significant at $P \leq 0.05$. *Significant from air-exposed controls at $P < 0.05$; #significant from ECV-0 at $P < 0.05$; @significant from ECV-6 at $P < 0.05$; $significant from the same exposure at 16 wk at $P < 0.05$.

ECV Exposure Reduces NO Bioavailability

Since ECV exposure resulted in VED with decreased ACh-mediated relaxation, we expected that NO production would be decreased. To verify this, NO generation in aortic sections, which were stimulated with 1 μM ACh, was measured using the NO-sensitive fluorescent probe DAF-FM that reacts with NO and produces green fluorescence. In the aorta from the air-exposed mice, prominent green fluorescence was observed; however, with ECV exposure, this fluorescence intensity was decreased, with lowest levels seen in aortas of the 60-wk ECV-24-exposed group (Fig. 3, *A–C*). The NO-DAF-generated fluorescence was largely blocked when the NO scavenger C-PTIO was added before the DAF-FM. Intergroup statistical analysis was done as presented in Fig. 4*B*. These data show that ECV exposure decreased NO levels in the aorta in an exposure time- and a nicotine-dependent manner.

ECV Exposure Increases Superoxide Radical Production in the Aorta

ECV exposure has been previously reported to result in oxidative stress and superoxide production (30), which can react with NO, decreasing its bioavailability, as seen in Fig. 3. Therefore, we applied the fluorescent probe DHE (10 μM) to detect superoxide generation in sections from freshly harvested mouse aortic rings. As shown in Fig. 4, *A* and *B*, after 16 wk of exposure, the intensity of DHE fluorescence was higher in all ECV-exposed groups, compared with air-exposed controls, with the ECV-24 group showing the highest intensity (6.2-fold increase) ($P < 0.001$). A similar pattern was observed after 60 wk of ECV-0, ECV-6, and ECV-24 exposure, with a 2.7-, 6.7-, and 7.5-fold increase in fluorescence intensity, respectively, (all $P < 0.001$) compared with air-exposed controls. ROS-DHE-generated fluorescence was largely quenched when the ECV-24-exposed aorta was preincubated with the SODm MnTBAP (100 μM) before DHE, confirming that ECV-induced ROS is the source of the developed fluorescence. More complete statistical analysis between the groups and exposure times is presented in Fig. 4*B*.

ECV Exposure Increases Protein Nitration

To determine if the ECV exposure-induced superoxide generation is associated with NO scavenging leading to protein modification, we measured the levels of nitrotyrosine (NT) formed from peroxynitrite. Immunoblotting after 16 wk of exposure to ECV-0, ECV-6, or ECV-24 showed an increase

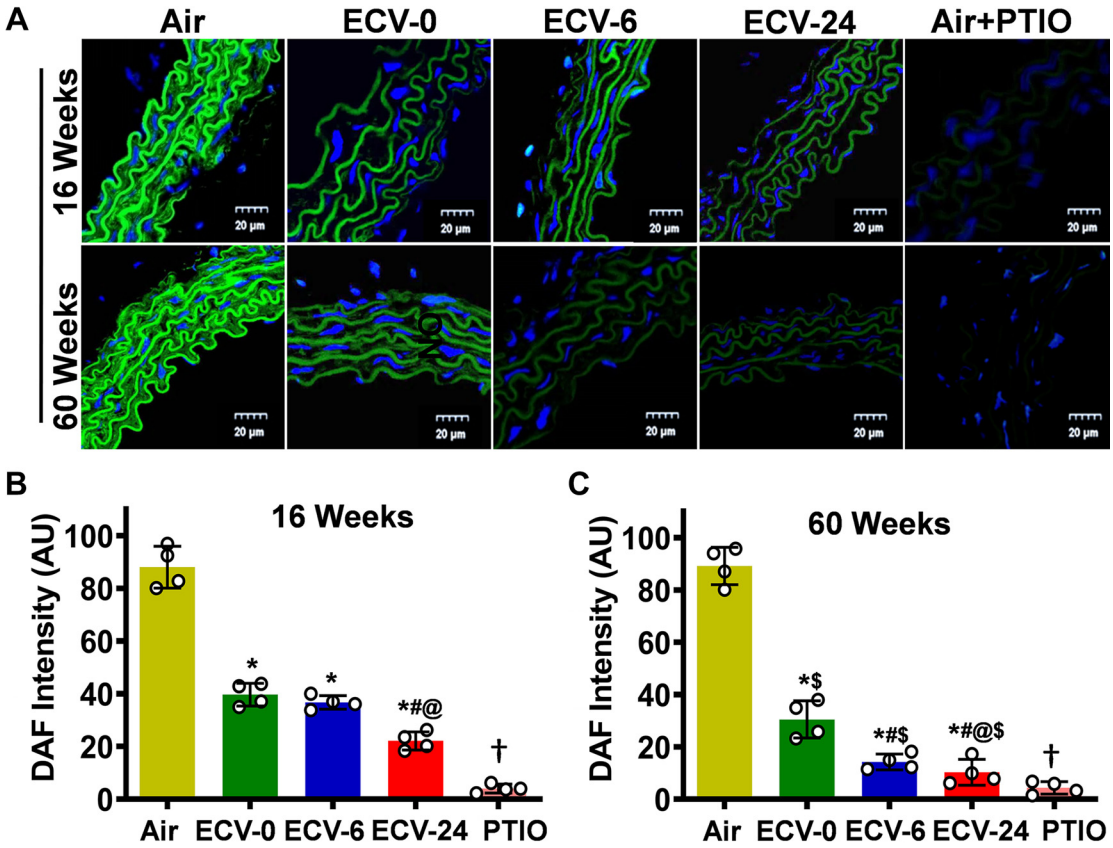

Figure 3. Nitric oxide (NO) bioavailability in the aorta. Aortic sections were studied from mice exposed to 16 and 60 wk of either air or electronic cigarette (e-cig) vape generated from e-cig liquid containing nicotine (NIC) 0 mg/mL (ECV-0), 6 mg/mL (ECV-6), or 24 mg/mL (ECV-24). *A*: sections were treated with the fluorescent nitric oxide (NO) probe diaminofluorescein-FM (DAF; green) and the nuclear fluorescent stain diamidino-2-phenylindole (DAPI; blue), with (air-exposed) or without the NO trap 2-(4-carboxyphenyl)-4,4,5,5-tetramethylimidazoline-1-oxyl-3-oxide (PTIO treated), and visualized by confocal fluorescence microscopy. A 20-μm scale bar is shown toward the lower right corner of each figure. *B* and *C*: quantitation of the green fluorescence in *A*. ECV exposure decreased NO levels in the aorta in an exposure time- and a NIC-dependent manner. Data show the means ± SE of aortic sections from 4 mice. Analysis was done using two-way ANOVA followed by Bonferroni multiple-comparisons test. The differences were considered statistically significant at $P \leq 0.05$. *Significant from air-exposed controls at $P < 0.05$; #significant from ECV-0 at $P < 0.05$; @significant from ECV-6 at $P < 0.05$; $significant from the same exposure at 16 wk at $P < 0.05$; †significant difference from ECV-24 in the absence of PTIO at $P < 0.05$.

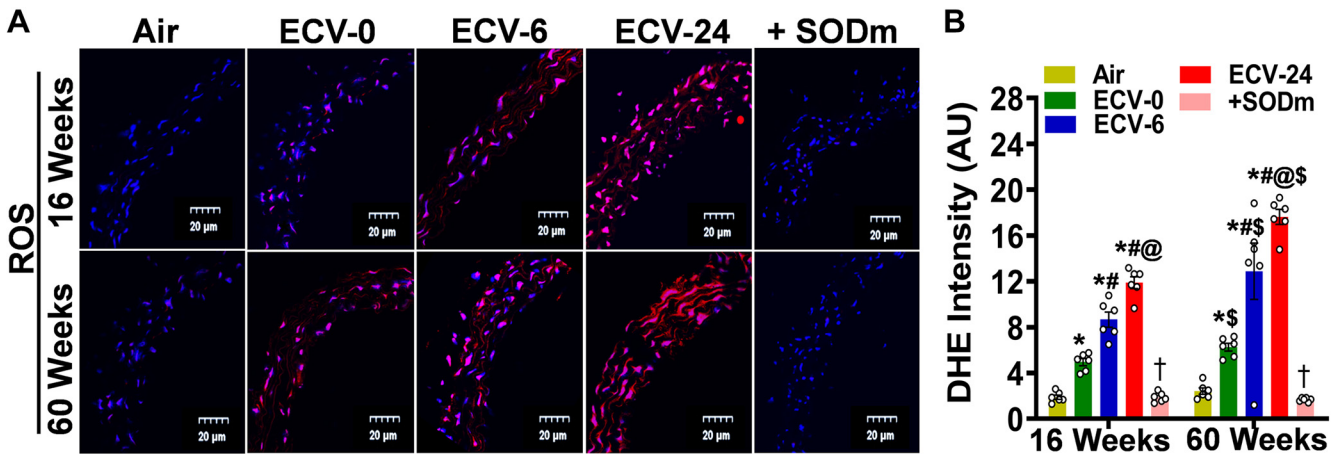

Figure 4. Superoxide radical generation in aorta. Aortic sections from mice exposed to 16 and 60 wk of either air or electronic cigarette (e-cig) vape generated from e-cig liquid containing nicotine (NIC) 0 mg/mL (ECV-0), 6 mg/mL (ECV-6), or 24 mg/mL (ECV-24) were studied. *A*: incubated with the superoxide probe dihydroethidium (DHE; red) and the nuclear fluorescent stain diamidino-2-phenylindole (DAPI; blue), with or without the superoxide dismutase mimetic Mn(III)tetrakis(4-benzoic acid)porphyrin chloride (+SODm), and imaged with confocal fluoroscopy. *B*: quantitation of the red fluorescence in *A*, showing that ECV exposure induced superoxide generation that was quenched by the SODm. Thus, ECV exposure results in vascular superoxide production in an exposure time- and a NIC-dependent manner. Data represent means ± SE of aortic sections from 6 mice. Analysis was done using two-way ANOVA followed by Bonferroni multiple-comparisons test. The differences were considered statistically significant at $P \leq 0.05$. *Significant from air-exposed controls at $P < 0.05$; #significant from ECV-0 at $P < 0.05$; @significant from ECV-6 at $P < 0.05$; $significant from the same exposure at 16 wk at $P < 0.05$; †significant from ECV-24 in the absence of the SODm at $P < 0.05$. ROS, reactive oxygen species.

in NT levels by 1.8-, 2.6-, or 3.3-fold, respectively (all $P <$ 0.05), compared with air-exposed controls (Fig. 5, *A–D*). Extending the exposure to 60 wk resulted in 2, 4 and 5.3-fold increase of NT levels in the aortas of ECV-0-, ECV-6-, and ECV-24-exposed mice, respectively (all $P < 0.04$), compared with the air-exposed control group. These results were confirmed by immunofluorescence microscopy, where the intensity of NT-derived fluorescence clearly increased in all ECV exposure groups, compared with air-exposed control (Fig. 5*E*). After 60 wk of exposure to ECV-0, ECV-6, or ECV-24, 3, 4 or 6.3-fold, respectively, (all $P < 0.03$) increases in nitrotyrosine levels were observed, compared with air-exposed controls (Fig. 5*F*). These data suggest that ECV-generated superoxide scavenged NO, leading to production of cytotoxic peroxynitrite that reacts to nitrate tyrosine in a broad range of proteins. It further confirms that the ECV-induced increase in vascular superoxide generation decreases NO bioavailability with the production of reactive nitrogen species, which together contribute to the onset of VED. More complete statistical analysis between the groups and exposure times is presented in Fig. 5, *C*, *D*, and *F*.

ECV Exposure Decreases eNOS Expression and Phosphorylation in the Aorta

eNOS plays a major in endothelial NO generation, and its levels are critical for NO synthesis. The process of eNOS activation is Ca^{2+}/calmodulin-dependent, and with eNOS phosphorylation at serine 1177 (p-eNOS^{ser1177}), the activation occurs at lower Ca^{2+} levels (40, 41). Therefore, we investigated the impact of ECV exposure on eNOS expression and phosphorylation. Western blot analysis revealed that 16 wk of ECV-0 or ECV-6 exposure was sufficient to downregulate the eNOS expression and was also associated with lower levels of p-eNOS^{ser1177}; however, these effects were more prominent with ECV-24 exposure and also after 60 wk of exposure (Fig. 6, *A–F*). As shown in Fig. 6*C*, after 16 wk of exposure to ECV-0, ECV-6, or ECV-24, eNOS expression decreased to 50, 30, or 15%, respectively, of the basal levels present in the air control vessels (all $P < 0.003$). Extending the exposure to 60 wk (Fig. 6*D*) resulted in further decrease of eNOS to 80% ($P < 0.05$), 17% ($P <$ 0.002), or 12% ($P < 0.001$), respectively, of the levels in the matched air control aortas. The levels of p-eNOS^{ser1177} following 16 wk of ECV-0, ECV-6, and ECV-24 exposure decreased to 90% ($P < 0.059$), 40% ($P < 0.031$), or 8% ($P < 0.001$), respectively, of the levels in air-exposed controls (Fig. 6*E*). After 60 wk of exposure, further decrease in the levels of p-eNOS^{ser1177} were seen (Fig. 6*F*). Thus, ECV exposure was associated with decreased levels of eNOS and p-eNOS^{ser1177} in all groups but was increased in the presence of higher NIC levels.

Akt is the major kinase responsible for the phosphorylation of eNOS at serine ^{1177}; therefore, we performed immunoblotting to measure the effects of ECV on the activation of Akt. Western blotting showed that ECV exposure decreased the Akt phosphorylation at Ser473, which is associated with Akt activation (Fig. 6, *G* and H), with this decrease paralleling that of p-eNOS^{ser1177} (Fig. 6, *E* and F). Akt phosphorylation was decreased after 16 wk of ECV-0, ECV-6, or ECV-24 exposure by 10% ($P = 0.057$), 25% ($P < 0.05$), or 97% ($P <$ 0.001), respectively, whereas further decreases of 44% ($P <$ 0.004), 83% ($P < 0.0001$), or 97% ($P < 0.0001$), respectively, were observed after 60 wk of exposure. Thus, both decreased Akt activation and lower eNOS levels contribute to the decline in p-eNOS^{ser1177} levels and the loss of vascular NO synthesis observed with ECV exposure.

To confirm the alterations observed for eNOS and p-eNOS^{ser1177} levels, immunohistology studies were performed with fluorescence detection of eNOS and p-eNOS in aortic sections after 60 wk of exposure. As expected, both eNOS and p-eNOS^{ser1177} were localized to the endothelium of the vessels (Fig. 6I). With ECV exposure, both eNOS and p-eNOS^{ser1177} levels were decreased in all ECV-exposed groups, compared with air-exposed controls. These experiments demonstrate

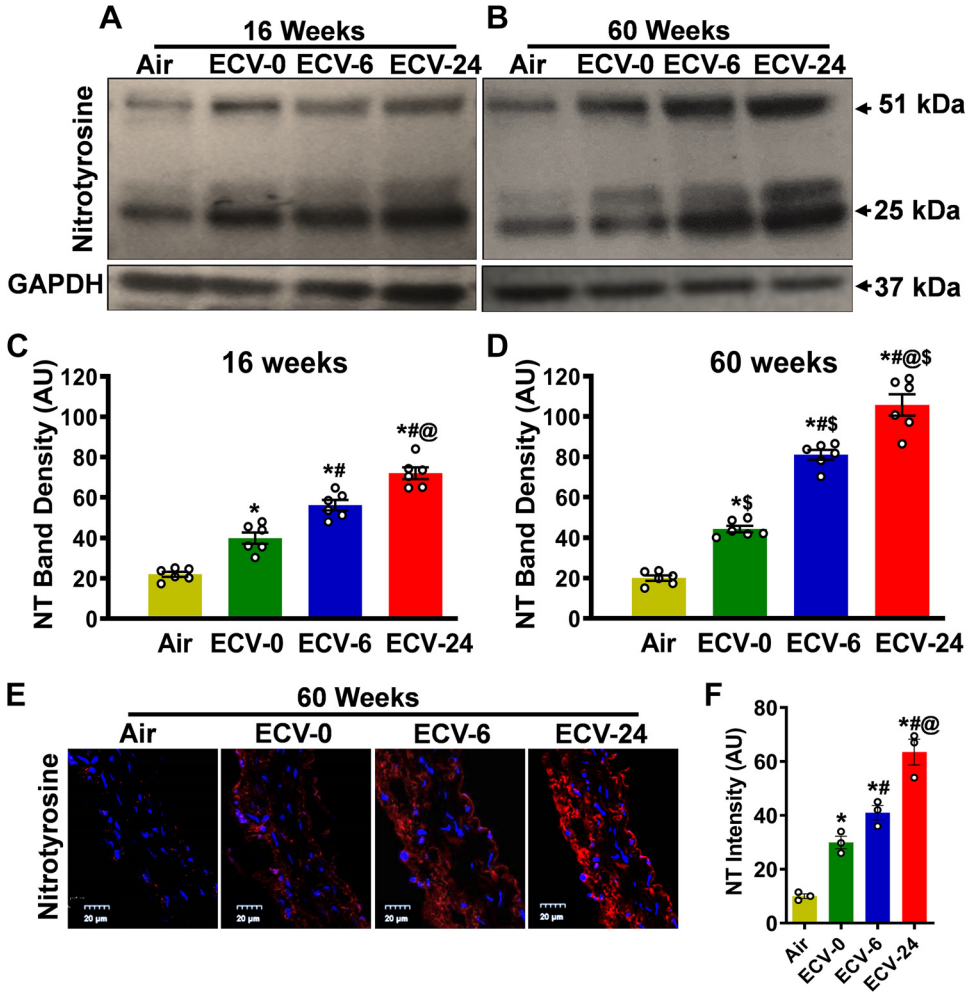

Figure 5. Nitrotyrosine formation in aorta. Nitrotyrosine (NT) levels were measured by Western blotting in aortic homogenates (*A–D*) and by immunofluorescence in aortic sections (*E* and *F*) from mice exposed to 16 or 60 wk of either air or electronic cigarette (e-cig) vape generated from e-cig liquid containing nicotine (NIC) 0 mg/mL (ECV-0), 6 mg/mL (ECV-6), or 24 mg/mL (ECV-24). *A* and *B*: immunoblots of NT levels. *C* and *D*: quantitation of NT bands in *A* and *B*, respectively, showing increased NT in a time- and NIC-dependent manner. *E*: aortic sections were incubated with primary antibody against NT followed by corresponding fluorescent labeled secondary antibody (red). The fluorescent dye diamidino-2-phenylindole (DAPI; blue) was used as a nuclear stain. *F*: quantitation of red fluorescence in *E*, showing similar effects as in *C* and *D*. These data indicate that ECV-generated superoxide scavenges nitric oxide (NO) producing cytotoxic peroxynitrite, with loss of NO bioavailability and ECV-induced VED. For *C* and *D*, data are presented as means ± SE with measurements performed in 6 mice. In *F*, each point is derived from measurements in 3 mice. Analysis was done using two-way ANOVA followed by Bonferroni multiple-comparisons test. The differences were considered statistically significant at $P \leq 0.05$. *Significant from air-exposed controls at $P < 0.05$; #significant from ECV-0 at $P < 0.05$; @significant from ECV-6 at $P < 0.05$; $significant from the same exposure at 16 wk at $P < 0.05$.

that ECV exposure and the VED that it triggers are associated with major endothelial loss of eNOS and p-eNOS^{ser1177}, such that endothelial NO synthesis would be decreased. Detailed statistical comparisons are presented in Fig. 6, *C–H*.

ECV Exposure Increases Endothelial NADPH Oxidase Expression and Superoxide Generation

Since we observed that ECV exposure triggers superoxide production, which was associated with superoxide-mediated decrease in NO bioavailability, as well as loss of eNOS expression and function, we aimed to identify the mechanisms of ECV-induced superoxide generation in the endothelium. First, we tested whether ECV alters the levels of NADPH oxidase in the aorta, which can serve as a major source for superoxide in the endothelium. As shown in Fig. 7, *A* and *C*, after 16 wk of exposure to ECV-0, ECV-6, and ECV-24, NADPH oxidase (NOX2) expression increased by 1.6-, 1.8-, and 2.3-fold, respectively, all significant at $P < 0.05$, compared with air-exposed controls. Moreover, with 60 wk of exposure, the expression of NOX-2 was further increased in each exposure group, with a maximum of 5.6-fold ($P < 0.005$) increase in the ECV-24 group, compared with air-exposed controls (Fig. 7, *B* and *D*). These Western blot results were further confirmed by immunofluorescence measurements, which additionally enables visualization of the localization of NOX2 within the vessel. From the observed fluorescence, NOX2-derived fluorescence was clearly increased in the aorta of ECV-exposed mice, with the ECV-24 group showing the highest intensity, with approximately sevenfold increase ($P < 0.0001$). In all NOX-2 immunofluorescence images, maximum fluorescence was seen in the endothelium, with a much weaker fluorescence throughout the vessel wall (Fig. 7*E*).

Further experiments were performed to measure the contribution of NADPH oxidase to the process of ECV-induced superoxide generation in ECV-exposed aortas. The aortic sections were preincubated with the specific pan-NADPH oxidase inhibitor VAS2870 before the addition of DHE (Fig. 7*G*). As shown in Fig. 7*H*, VAS2870 largely decreased the DHE-superoxide-generated fluorescence by 78% and 80% ($P < 0.001$) in the 16- and the 60-wk ECV-24 exposure group, respectively. In addition, the NOX2-specific NADPH oxidase inhibitor GSK2795039 markedly decreased the DHE fluorescence by 84% and 83% ($P < 0.0001$) in the 16- and the 60-wk ECV-24 exposure groups, respectively. Taken together, these results indicate that induction of NOX2 in the endothelium is a major source of ECV-stimulated superoxide seen in all ECV-exposed groups. This induction increased with exposure duration and e-cig NIC content. More robust statistical analysis was done to compare means among groups. Detailed intergroup comparisons are presented in Fig. 7*F*.

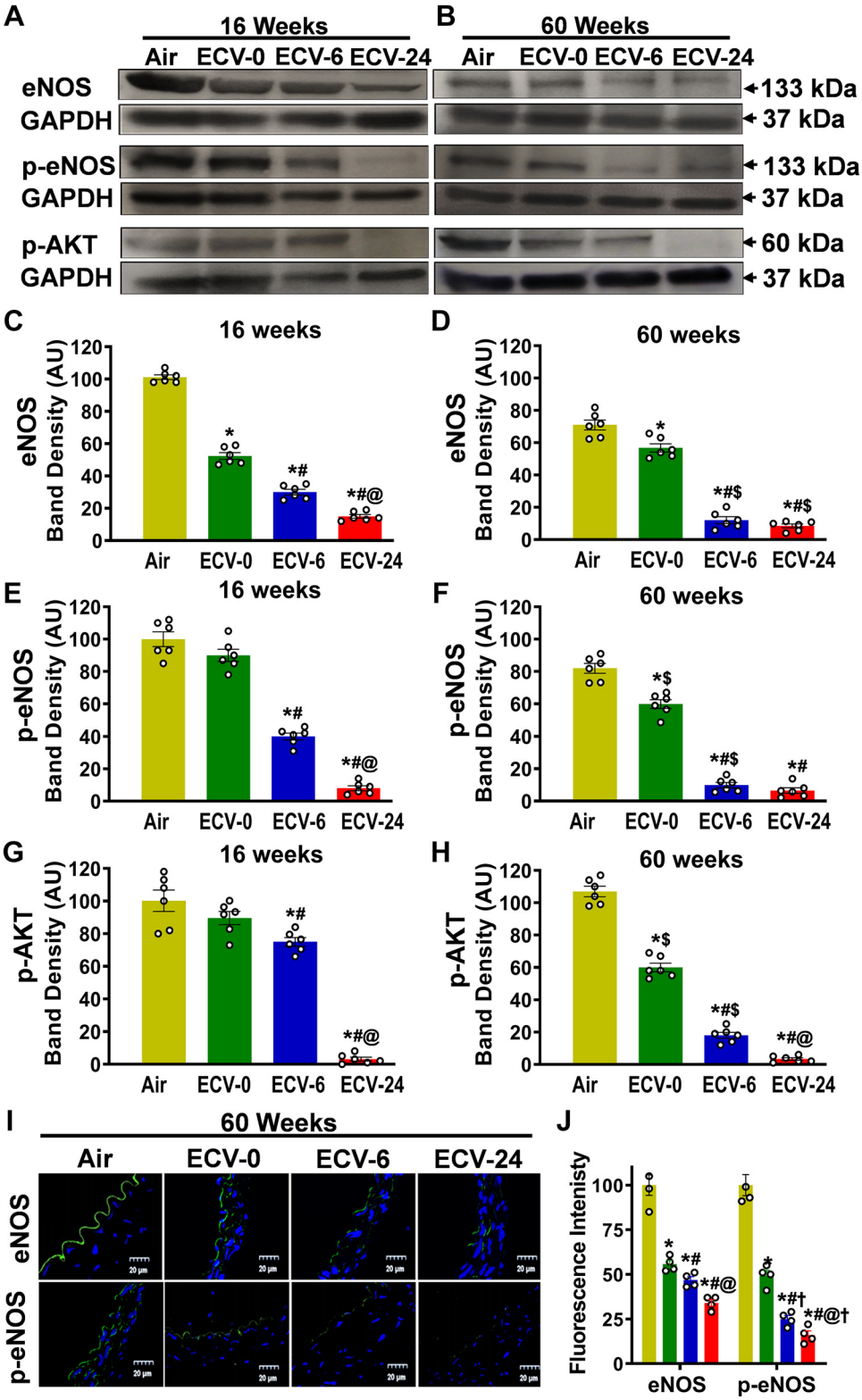

Figure 6. Endothelial nitric oxide (NO) synthase expression and phosphorylation in aorta. *A* and *B*: Western blotting was used to measure the expression and phosphorylation of endothelial nitric oxide synthase (eNOS) and phosphorylation of AKT (p-AKT) in the aorta from mice exposed to 16 and 60 wk of either air or electronic cigarette (e-cig) vape generated from liquid containing nicotine (NIC) 0 mg/mL (ECV-0), 6 mg/mL (ECV-6), or 24 mg/mL (ECV-24). *C* and *D*: quantitation of eNOS bands in *A* and *B*, respectively, showing downregulation of e-NOS in an exposure time- and NIC-dependent manner. *E* and *F*: quantitation of p-eNOS bands in *A* and *B*, respectively, showing similar decreases as in *C* and *D*. *G* and *H*: quantitation of p-AKT bands in *A* and *B*, respectively, also exhibiting similar decreases. *I*: frozen aortic sections were incubated with primary antibody against eNOS and p-eNOS followed by corresponding secondary fluorescence antibody (green) and the nuclear stain DAPI (blue). *J*: quantitation of green fluorescence of eNOS and p-eNOS. ECV exposure downregulated eNOS expression and decreased Akt-dependent eNOS phosphorylation, contributing to the decline of NO synthesis and onset of VED. Data are presented as means ± SE of 6 exp-eriments. For *C*–*H*, data are presented as means ± SE of independent experiments in 6 mice, whereas for *J*, each point is based on independent experiments in 4 mice. Analysis was done using two-way ANOVA followed by Bonferroni multiple-comparisons test. The differences were considered statistically significant at $P \leq 0.05$. *Significant from air-exposed controls at $P < 0.05$; #significant from ECV-0 at $P < 0.05$; @significant from ECV-6 at $P < 0.05$; $significant from the same exposure at 16 wk at $P < 0.05$. †significant different from eNOS expression at $P < 0.05$.

ECV Exposure Triggers eNOS Uncoupling, Depletes BH_4, and Downregulates DHFR

We further tested whether ECV triggers NOS-uncoupling, which has been identified as another critical mechanism of superoxide generation, triggered by oxidant stress (42–44). In NOS-uncoupling, eNOS function as an NO synthase is disrupted, leading to the production of superoxide instead of NO (44). We assessed the role of NOS in ECV-induced superoxide generation by testing the effect of the NOS

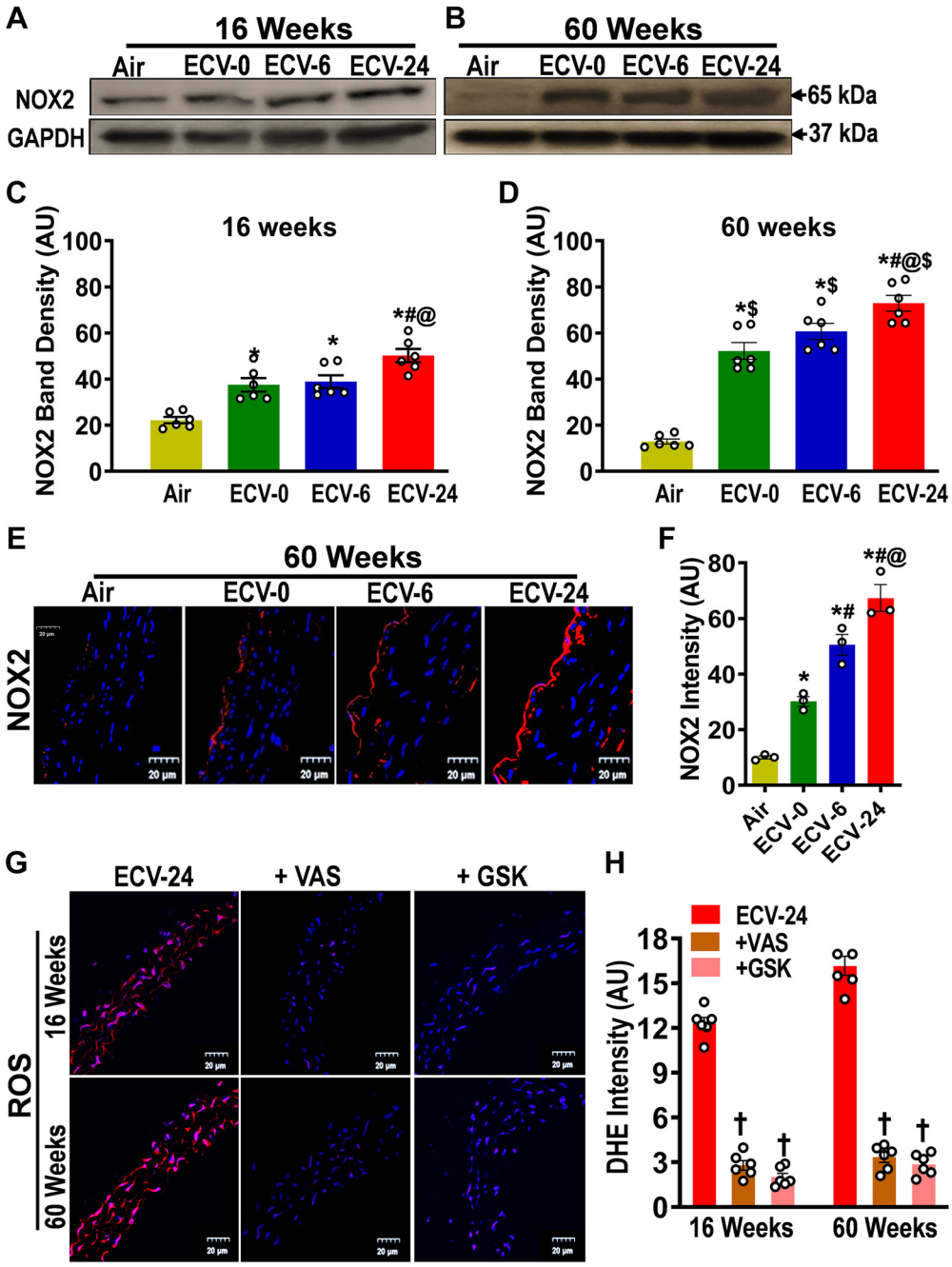

Figure 7. Expression of NADPH oxidase 2 in the aorta. NADPH oxidase 2 (NOX2) levels were measured by Western blotting (*A*–*D*) and immunofluorescence (*E* and *F*) from mice exposed to 16 and 60 wk of either air or electronic cigarette (e-cig) vape generated from liquid containing nicotine (NIC) 0 mg/mL (ECV-0), 6 mg/mL (ECV-6), or 24 mg/mL (ECV-24). *A* and *B*: immunoblots of NOX2. *C* and *D*: quantitation of NOX2 band density in *A* and *B*, respectively, showing exposure time- and NIC-dependent increases in NOX2 expression. *E*: aortic sections were incubated with primary antibody against NOX2 followed by corresponding secondary fluorescent tagged antibody (red), with DAPI nuclear stain (blue). *F*: quantitation of red fluorescence in *E*, showing a similar response as in *D*. *G*: aortic sections from ECV-24-exposed mice were incubated with the superoxide probe dihydroethidium (DHE; red) and DAPI (blue), with or without NADPH oxidase inhibitors 3-benzyl-7-(2-benzoxazolyl)thio-1,2,3-triazolo[4,5-d]pyrimidine (+VAS) or GSK2795039 (+GSK), and visualized by confocal microscopy. *H*: quantitation of the superoxide-derived red fluorescence in *G*, showing that NOX2 inhibitors decreased superoxide in ECV-24-exposed aortic sections. Thus, induction of NOX2 in the endothelium is a major source of the ECV-stimulated superoxide seen in all ECV-exposed groups, and its induction increased with exposure duration and NIC content. For *C* and *D*, data are presented as means ± SE of 6 mice, whereas for *F* and *H*, $n = 3$ or 6 mice, respectively. Analysis was done using two-way ANOVA followed by Bonferroni multiple-comparisons test. The differences were considered statistically significant at $P \leq 0.05$. *Significant from air-exposed controls at $P < 0.05$; #significant from ECV-0 at $P < 0.05$; @significant from ECV-6 at $P < 0.05$; $significant from the same exposure at 16 wk at $P < 0.05$. †significant different from ECV-24-exposed sections stained with DHE.

inhibitor L-NAME on the overall generation of superoxide by ECV. As seen in Fig. 8, *A* and *B*, preincubation of the aorta with L-NAME reduced DHE-superoxide-generated fluorescence by 63% and 64% ($P < 0.005$) in 16- and 60-wk ECV-24-exposed aortas, respectively, compared with ECV-24-exposed controls (no L-NAME preincubation). Figure 8, *C* and *D*, shows that ECV exposure depleted the redox-sensitive eNOS cofactor BH_4. BH_4 levels significantly decreased from 1.5 ± 0.02 pmol/mg protein in the air-control group to 0.9 ± 0.09, 0.87 ± 0.09, and 0.73 ± 0.07 pmol/mg protein ($P < 0.05$) in the ECV-0, ECV-6, and ECV-24 groups, respectively, after 16 wk of exposure. Further declines were observed following 60 wk of exposure, with values of 0.66 ± 0.08, 0.60 ± 0.06, and 0.54 ± 0.04 pmol/mg protein ($P < 0.005$) in the ECV-0, ECV-6, and ECV-24 groups, respectively, compared with the air-exposed control group. Figure 8, *E* and *F*, shows that ECV exposure downregulated dihydrofolate reductase (DHFR), the key enzyme responsible for the salvage of BH_4 from BH_2. Similar to BH_4, 16 wk of exposure to ECV-0, ECV-6, or ECV-24 significantly downregulated the expression of DHFR by 65%, 70%, and 95% (all $P < 0.001$), respectively. Exposure to 60 wk of ECV-0, ECV-6, or ECV-24 further decreased the expression by 75%, 85%, and 90% (all $P < 0.0001$), respectively (Fig. 8, *G* and *H*). Thus, these results indicate that eNOS uncoupling occurs and is an important source of ECV-induced superoxide generation. Detailed intergroup comparisons with statistical analysis are presented in Fig. 8, *C, D, G,* and *H*.

DISCUSSION

This study extends our recent work where we developed a mouse model of chronic vaping-induced cardiovascular dysfunction and hypertension (30, 34). Herein, we utilized this model to investigate the underlying mechanisms in the pathogenesis of ECV-induced VED

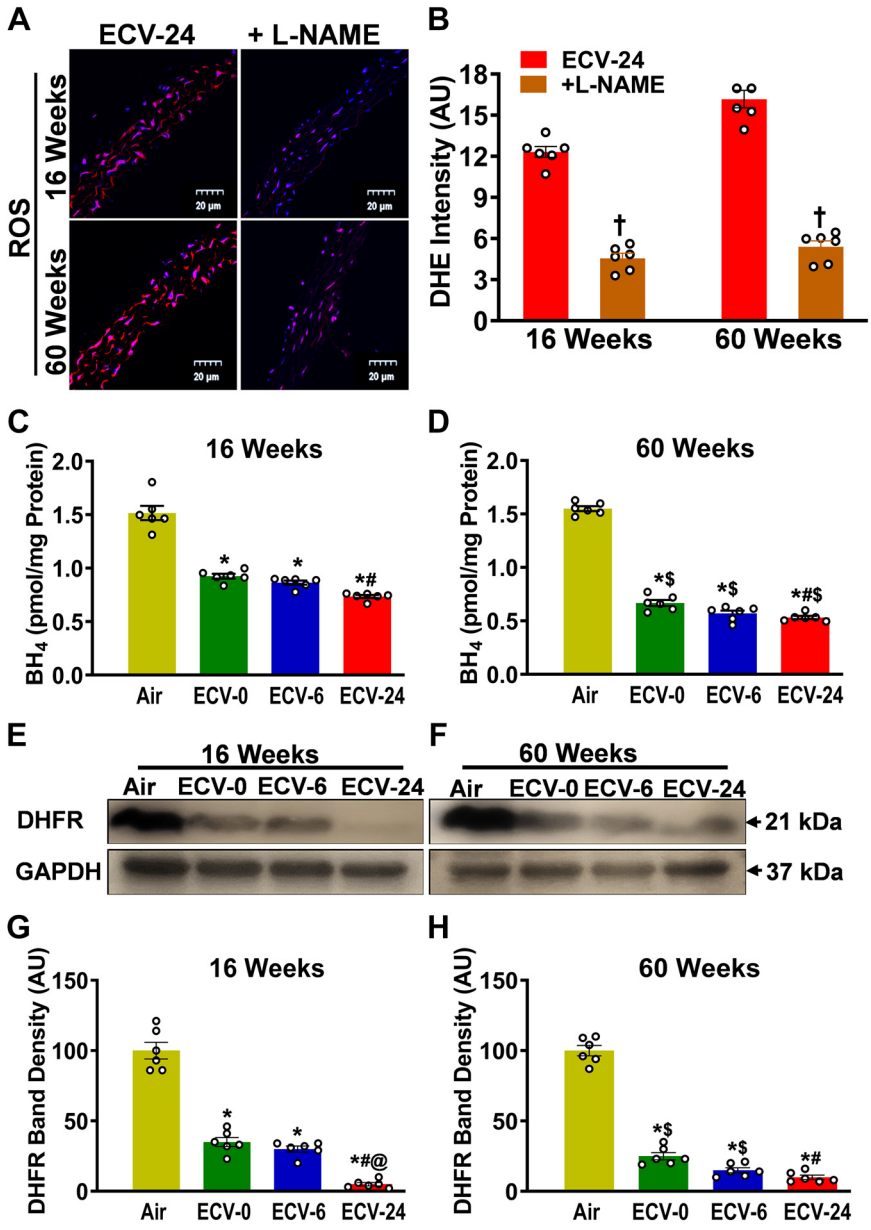

Figure 8. Nitric oxide synthase uncoupling in the aorta. *A*: aortic sections from ECV-24-exposed mice were incubated with the superoxide probe dihydroethidium (DHE; red) and DAPI (blue), with or without nitric oxide synthase inhibitor L-NAME. *B*: quantitation of fluorescence in *A*, showing that L-NAME decreased the DHE fluorescence in ECV-24-exposed aortic sections. *C* and *D*: ELISA quantitation of aortic tetrahydrobiopterin (BH_4) following either air or electronic cigarette (e-cig) vape generated from e-cig liquid containing nicotine (NIC) 0 mg/mL (ECV-0), 6 mg/mL (ECV-6), or 24 mg/mL (ECV-24). *E* and *F*: immunoblots of DHFR expression. *G* and *H*: quantitation of band density in *E* and *F*, respectively, showing exposure time- and NIC-dependent downregulation of DHFR. Thus, NOS is a source of ECV-induced superoxide with ECV depleting BH_4 and DHFR, leading to eNOS uncoupling. For *B*, *C*, *D*, *G*, and *H*, data are presented as means ± SE of values from 6 mice. Analysis was done using two-way ANOVA followed by Bonferroni's multiple-comparisons test. The differences were considered statistically significant at $P \leq 0.05$. *Significant from air-exposed controls at $P < 0.05$; #significant from ECV-0 at $P < 0.05$; @significant from ECV-6 at $P < 0.05$; $significant from the same exposure at 16 wk at $P < 0.05$. †significant different from ECV-24 sections in the absence of L-NAME. DHFR, dihydrofolate reductase enzyme; eNOS, endothelial nitric oxide synthase; L-NAME, N^G-nitro-L-arginine methyl ester; NOS, nitric oxide synthase.

and cardiovascular disease. Our principal findings are as follows: *1*) ECV exposure decreases endothelium-dependent vasodilation and increases BP and SVR; *2*) the observed VED increases with extended exposure times and also with increased aerosol nicotine content but is still seen with ECV in the absence of nicotine; *3*) ECV-induced VED is accompanied by decreased NO levels and increased superoxide generation within the vascular wall; *4*) increased nitrotyrosine levels are detected in the vessels, indicating the formation of the potent oxidant peroxynitrite with secondary protein nitration; *5*) decreased eNOS and p-eNOS^{ser1177} levels were observed, contributing to the loss of NO and reduced endothelial vasodilation; *6*) increased expression of NOX2 occurs in the vessel and is an important source of ECV-induced superoxide, as demonstrated by superoxide generation inhibition by specific NOX inhibitors; *7*) decreased vascular BH_4 levels were seen with decreased levels of the BH_4 salvage enzyme DHFR; and *8*) furthermore, the NOS inhibitor L-NAME decreased vascular superoxide generation, indicating that eNOS uncoupling contributed to the ROS generation and loss of NO synthesis and bioavailability that occur with ECV-induced VED. Thus, we see that ECV exposure triggers vascular oxidant stress through induction and activation of NADPH oxidase and eNOS uncoupling, with both pathways generating superoxide, secondary ROS, and peroxynitrite, leading to a vicious cycle of ROS-induced ROS generation (Fig. 9).

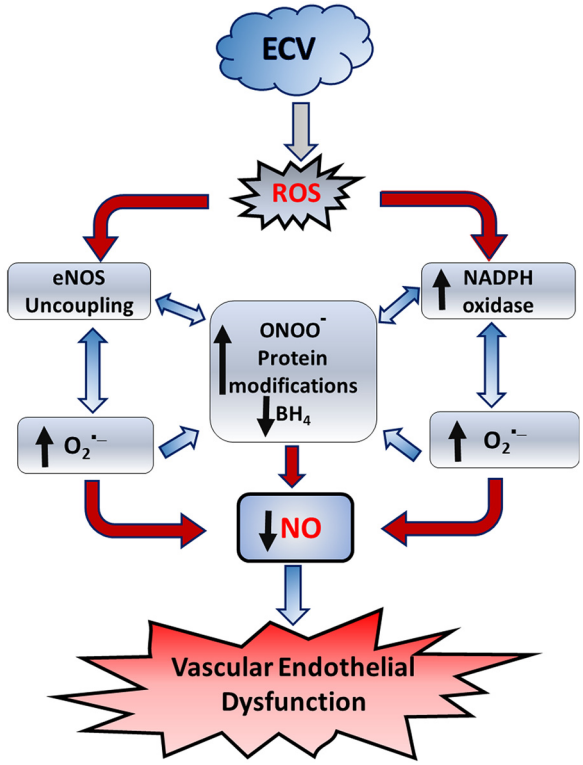

Figure 9. Process by which electronic cigarette vape (ECV) exposure triggers endothelial reactive oxygen species (ROS) generation and vascular endothelial dysfunction. ECV exposure generates ROS that increase the activation and expression of NADPH oxidase and trigger nitric oxide (NO) synthase (eNOS) uncoupling, leading to a vicious cycle of superoxide production and peroxynitrite formation, with protein modifications, and tetrahydrobiopterin (BH_4) depletion. Together these cause decreased NO synthesis and bioavailability, leading to endothelial dysfunction.

Design of the Exposure Model and Relevance to Human e-Cig Exposure

Our recently developed long-term controlled ECV exposure model in mice (30, 34) was designed to mimic the chronic exposure in human e-cig users. We designed this model to parallel the pattern of human tobacco smoking or e-cig usage. With regard to nicotine, as previously reported, the intensity of vaping exposure of the mice was tailored to match the blood levels of the major nicotine metabolite cotinine for the nicotine-containing groups (ECV-6, ECV-24) with matched aerosol exposure in the nicotine-free group (ECV-0) (34). With this exposure protocol as performed, the average particulate matter (TPM) was measured as 880 mg/m^3 in the 5-L exposure chamber, and plasma cotinine levels immediately following exposure were 64 ng/mL and 240 ng/mL for the 6 or 24 mg/mL groups, which is in the range measured in human smokers and e-cig users (45). With regard to age, most smoking or vaping users in the United States begin to smoke and use e-cig at 13–15 yr of age (~1/6th of life span) and continue smoking for decades. This starting age equates to 16 wk of age in mice (46). Therefore, we started exposures in mice of 16 wk of age. In our prior detailed longitudinal study (30), we observed significant vascular impairments as early as 16 wk of exposure and monitored disease progression, which reached a maximum at 60 wk. Accordingly, in the current mechanistic study, we aimed to investigate the underlying pathways at the exposure time points in which deterioration started of 16 wk and that of maximum severity of 60 wk (30).

E-Cig Exposure Triggers VED and HTN

Consistent with our prior study (30), mice exposed to ECV for 16 wk developed hypertension, and this was exacerbated with longer exposure durations with a 32 mmHg increase in MABP after 60 wk. Paralleling the rise in BP, SVR was increased in an exposure duration- and nicotine content-dependent manner. Our results are also consistent with the prior study of Olfert *et al.* (32), which observed the development of cardiovascular disease with chronic 32-wk exposure to ECV (18 mg/mL nicotine). The earlier onset and the more aggressive disease development in our model may reflect the efficient aerosol delivery with higher uptake by the mice, confirmed by monitoring of the plasma cotinine levels, which were measured to be comparable with those in human e-cig users (30, 34).

VED is associated with hypertension and cardiovascular disease onset and may precede their development (39). In the current study, we longitudinally monitored the BP and vascular response changes in the ECV-exposed mice throughout the 60 wk of exposure. At 16 wk of exposure, significant elevations in SBP, DBP, and MABP were seen in all ECV-exposed groups and BP further increased as a function of exposure duration out to 60 wk. We previously observed that large and small vessels from similar groups of ECV-exposed mice exhibited VED akin to that seen with

TC smoke exposure (30). In the current studies, similar alterations in endothelial-dependent relaxation were first observed in the aortas of ECV-6 and ECV-24 mice exposed to 6 or 24 mg/mL nicotine-containing e-cig aerosol after 16 wk of exposure. With further prolonged exposure of 60 wk, all exposed groups, including those with 0 mg/mL nicotine, exhibited VED compared with matched air control mice. These findings are similar to those of our prior study (30) and highlight the potential cardiovascular consequences of e-cigarette use, in opposition to earlier claims regarding the safety of these products (47, 48). Similar to endothelium-dependent relaxation, the endothelium-independent relaxation was also impaired with ECV exposures; however, as expected, consistent with prior reports, the magnitude of this dysfunction was lower (30). Thus, although the major loss of vasodilation was endothelium-dependent, there is also significant loss of endothelium-independent relaxation that could be caused by a decrease in NO bioavailability due to scavenging by superoxide or other pathways of NO degradation (6, 49).

E-Cig Exposure Triggers Loss of NO Bioavailability

Lack of NO bioavailability is central to the onset of VED (2). In normal conditions, a delicate balance between NO synthesis and breakdown preserves the physiological levels of NO and maintains vascular homeostasis; however, this balance is disrupted in cardiovascular diseases, such as hypertension, atherosclerosis, and coronary artery disease (50). We observed marked reductions in NO levels measured in the vascular wall following ECV exposure, which were exacerbated with longer exposure duration or higher aerosol nicotine levels. Beyond the loss of the vasodilatory function, lack of NO bioavailability also leads to impairments in the anti-inflammatory, antiplatelet, and antiapoptotic functions (1). The lack of intravascular NO bioavailability is due to a combination of decreased synthesis by eNOS and increased breakdown secondary to elevated levels of superoxide generation or enhanced vascular NO metabolism.

Vascular oxidative stress triggers a lack of NO bioavailability and consequently predisposes to cardiovascular disease (51). Exposure to ECV for 16 or 60 wk resulted in increased superoxide generation with larger increases with higher aerosol nicotine content. Superoxide is a short-lived free radical that reacts with NO by a diffusion-controlled reaction resulting in the formation of peroxynitrite (52). This cytotoxic peroxynitrite mediates oxidative modifications in biomolecules such as protein tyrosine nitration, which results in altered protein structure and function. Peroxynitrite-induced protein tyrosine nitration is recognized by the formation of 3-nitrotyrosine (53), which is proposed as a biomarker for various cardiovascular diseases such as atherosclerosis, myocardial ischemia, and hypertension (49, 54). We observed elevated levels of 3-nitrotyrosine in aortic homogenates of mice exposed to ECV. In conventional smoking, high 3-nitrotyrosine levels were detected (55) and correlated with the progression of chronic obstructive pulmonary disease in smokers (56). The current study is the first, to our knowledge, to detect 3-nitrotyrosine production in vessels following ECV exposure, demonstrating the role of vascular superoxide in depleting NO leading to VED.

Loss of eNOS Expression and Phosphorylation-Mediated Activation

Besides increasing the breakdown of NO, superoxide and secondary ROS might also impair NO synthesis due to loss of enzyme activity or degradation of the enzyme. We observed major decreases in eNOS levels following ECV exposure, further exacerbated with extended exposure and higher nicotine content, with the 60-wk-exposure ECV-24 group exhibiting >60% loss of eNOS on immunohistology and Western blotting. This reduced eNOS expression may be due to its degradation following oxidative modification by ECV-generated ROS and peroxynitrite. Indeed, we have previously shown that peroxynitrite, at high concentrations, irreversibly destroys the heme center of eNOS (57). It has also been shown that exposure of endothelial cells to tobacco cigarette extract stimulates proteasomal degradation of eNOS (58).

In addition to the decrease in total eNOS expression, ECV inhibited eNOS phosphorylation at Ser^{1177} even to a greater extent. Lower levels of p-Akt were seen presumably due to inhibition of the activity of Akt kinase. eNOS phosphorylation at Ser^{1177} is a mechanism that stimulates NO production at lower calcium levels (40, 59). Several kinases share the ability to phosphorylate this site, including protein kinase A, protein kinase C, CAMKII, and the serine/threonine kinase Akt. Akt is an essential checkpoint for eNOS activation in response to many signal transduction pathways (60). Dysregulation in Akt activity is associated with VED development in hypertension (61). Thus, the reduced phosphorylation of Akt at Ser473 suggests that an Akt-dependent pathway contributes to the decrease of eNOS activity. This reduction in active p-Akt might be attributed to oxidative modifications induced by ECV-generated superoxide or peroxynitrite. Similar results were obtained in our prior work on TC smoking exposure, where superoxide generation resulted in the downregulation of eNOS expression and reduced its Akt-mediated phosphorylation (27).

Sources of e-Cig-Stimulated ROS, Role of NADPH Oxidase, and Uncoupled eNOS

With the heating of the e-liquid by the e-cig atomizer, toxic free radicals and aldehydes are formed in the aerosol (62, 63), which could trigger oxidative injury not only in the lung and pulmonary circulation but also in the systemic circulation. In addition to primary e-cig-generated oxidants, there is growing evidence that ECV exposure activates the enzymatic production of ROS (64). We observed that two enzymatic systems, namely, NADPH oxidase and uncoupled NOS, serve as important sources of ECV-generated superoxide in the vascular endothelium.

NADPH oxidase is the predominant source of ROS in the vasculature, and it is activated in several animal models of vascular diseases, such as angiotensin II-induced hypertension (65), diabetes mellitus (66), and hypercholesterolemia (67). Moreover, NADPH oxidase activation is a likely cause of oxidative stress in hypertension-associated target organ damage (68, 69). We observed that ECV exposure increased NOX2 expression in a nicotine content- and exposure duration-dependent manner, where exposure to ECV-24 for 60 wk resulted in a sevenfold increase. The NADPH oxidase

inhibitors VAS or GSK decreased ECV exposure-generated superoxide by 78%–84%. These results confirm the role of NADPH oxidase in triggering oxidative stress in ECV users. Consistent with these findings, a recent study on short-term ECV consumption demonstrated NADPH oxidase as a key source of ECV-induced ROS, where NOX2-deficient mice did not develop oxidative stress or VED (70). Similarly, our previous studies on conventional TC smoking revealed the activation of superoxide generation by NADPH oxidase in mice (30).

Uncoupled eNOS is another critical source of superoxide in the endothelium and can be triggered by depletion of the obligate eNOS cofactor BH_4, which uncouples electron flow from L-arginine oxidation and leads to the production of superoxide instead of NO. BH_4 levels are affected by its de novo synthesis and the recycling of its oxidized form BH_2 to BH_4 by dihydrofolate reductase (DHFR) at the expense of NADPH (71). eNOS uncoupling is implicated in the pathogenesis of multiple cardiovascular diseases, including atherosclerosis (72), hypertension (73), and diabetes (74). The decreased level of BH_4 observed with ECV exposure together with the clear decrease in superoxide production by L-NAME indicates the contribution of eNOS uncoupling to the overall generation of superoxide. Furthermore, the reduced expression of DHFR indicates partial loss of the ability to salvage BH_4 from its oxidized form BH_2. ECV-induced oxidative stress would be expected to cause BH_4 oxidation. Of note, although direct BH_4 oxidation by superoxide is relatively slow (75), it is rapidly oxidized by peroxynitrite to BH_2 (57). Moreover, the observed reduction in DHFR might be attributed to peroxynitrite, which was found to trigger 20S peroxisome-mediated degradation of DHFR (76). Taken together, oxidative stress-induced eNOS uncoupling would result in a further increase in ROS generation, contributing to further uncoupling and triggering a vicious circle of ROS-induced ROS generation and secondary oxidative damage (Fig. 8).

Mechanisms of ROS Formation and Their Cross Talk

eNOS is central to endothelial vasodilator function, oxidizing NADPH with conversion of L-arginine and O_2 to citrulline and NO. The classical leukocyte NADPH oxidase NOX2 has also been shown to have a critical role in endothelial function, hypertension, and cardiovascular disease. Both have been previously demonstrated to be of central importance in tobacco smoking-induced VED (77). In endothelial cells, intracellular ROS are generated from several different sources including NADPH oxidases, uncoupled eNOS, mitochondria, cyclooxygenase, lipoxygenase, aldehyde oxidase, and xanthine oxidase (78). The role of cross talk between mitochondria and NADPH oxidases in endothelial cells has been reported in development of vascular endothelial dysfunction (79). The phenomenon of ROS-induced ROS release in mitochondria is well documented, first reported over 20 years ago (80, 81). Interactions with cross talk between endothelial, leukocyte, and cardiac smooth muscle cell processes of radical generation have been described and reviewed at length (78).

Although there are many possible sources of ROS, NADPH oxidases play a central role. NADPH oxidases are major sources of ROS in the vessel wall (82). There are seven isoforms of NADPH oxidases in mammals: NOX1, NOX2, NOX3, NOX4, NOX5, Duox1, and Duox2 (83). NOX2 is the main most highly expressed NOX in vessels both in endothelium and smooth muscle (82). NOX2 has been previously shown to have an important role in smoking-induced free radical generation and VED (27). In our initial experiments assaying superoxide in the vessels of ECV-exposed mice, we observed that a NOX2-specific inhibitor resulted in over 75% inhibition of superoxide generation. Therefore, in addition to characterizing alterations in eNOS expression and function, we focused our studies on assays of NOX2.

Role of Nicotine Content in e-Cig-Induced VED and Cardiovascular Disease

An important observation in the present study is the role of e-liquid nicotine content in the progression of VED and the underlying molecular mechanisms of oxidative stress. Although VED was observed with nicotine-free ECV exposure, the inclusion of nicotine exacerbated the VED and the observed oxidative stress. These findings clearly indicate that although nicotine is not the sole cause of the harmful effects of e-cig, it serves to heighten the harmful effects. Chronic nicotine administration was found to increase blood pressure, induce arterial remodeling, and impair endothelium-dependent relaxation (84, 85). Although the scope of the present study does not identify the mechanism of nicotine-induced oxidant stress, it is known that nicotine is metabolized in a process that can generate superoxide. Nicotine is metabolized by P450 to the nicotine-iminium ion, which is further metabolized by aldehyde oxidase to form superoxide and cotinine (86). In addition, the sympathomimetic activity of nicotine raises catecholamine levels that in turn autoxidize to form superoxide (87, 88).

Although, in the current work, nicotine content of e-cig liquid played a major role in the severity of VED observed, even in the absence of nicotine, VED was seen with prolonged exposure. In the ECV-0 group, although vascular reactivity and blood pressure changes did not reach significance with 16 wk of exposure, after 60 wk of exposure, clear highly significant changes were seen. We also observed similar results in our prior report, where NIC-free e-cig exposure induced pathological changes and NIC augmented these changes in a dose-dependent manner. Thus, it is clear that even NIC-free e-cig use can cause vascular dysfunction and cardiovascular disease in mice and possibly in humans with long-term use.

With acute NIC-free e-cig aerosol inhalation in healthy subjects, transient increase in oxidative stress and inflammation markers have been reported, suggesting that e-cig exposure without nicotine can drive the onset of vascular pathologies through ROS and immune cell activation (89). It is known that propylene glycol and glycerin, the main solvents in e-liquid, when aerosolized with heating, as occurs in the atomizer of e-cigs, can produce free radicals and volatile carbonyls such as acrolein, which are potent oxidative stressors (90). Furthermore, it has been shown that high doses of acetaldehyde and formaldehyde have harmful cardiovascular effects and accelerate atherosclerosis in vivo (91). Moreover, transition metals identified in e-cig emissions and the fine/ultrafine particles generated were found to catalyze ROS generation and local oxidative stress with induction of vascular

inflammation that contribute to endothelial damage and augment adrenergic activity, causing systemic HTN, stroke, and cardiac hypertrophy (88).

Effects of Aging

With chronic ECV exposure for prolonged periods, the animals inherently age, and this can contribute to the changes observed. VED develops with aging in humans in the absence of clinical cardiovascular disease (CVD) and major risk factors for CVD (92, 93). Endothelium-dependent vasodilatation progressively declines with age in both conduit and resistance vessels and occurs earlier in men than in women (94). Similar age-dependent changes in endothelium-dependent vasomotor responses have been reported in animal models. In particular, arteries from rats, pigs, rabbits, and mice showed decreased endothelium-dependent vasodilator responses with age, independent of structural changes in the vascular wall (94). This is in line with aging-associated vascular deteriorations that occur and are accompanied by oxidative stress-induced eNOS uncoupling (95). In our model, after 60 wk of exposure in mice of 76 wk of age, significant changes were seen in endothelial vasodilation in control air-exposed mice compared with that in 16-wk air-exposed, 32-wk-old mice, with 3.6-fold increase in the ACh dose required for 50% relaxation. However, much greater loss of endothelial function was seen in all the e-cig exposure groups at the 60 wk exposure duration, with over 18-fold increases in the required ACh dose for relaxation and large decreases in maximal relaxation. In parallel with this, significant decreases in the levels of eNOS and p-eNOS were seen in the air-control group with 60 wk exposure compared with that at 16 wk; however, in the ECV exposure groups, much larger decreases were seen. Thus, the effects of ECV exposure with onset of VED and eNOS impairment were much more severe than the effects of age alone; however, the inherently older age of the 60-wk-exposed mice could contribute to their marked susceptibility to oxidant-induced VED.

Limitations of the Current Study and Areas for Future Investigation

Although the current study provides important insights regarding the process and mechanisms by which chronic e-cig exposure triggers VED and CVD, there are multiple limitations and important areas for future study. With regard to sex, only male mice were studied, and there is a critical need for determination of the effects of sex on the mechanisms and process of e-cig-induced disease. There is also a need for studies regarding how the age of exposure onset affects subsequent disease. Another very important area is to determine how cessation affects VED and CVD severity and if disease is reversible. There is also a great need for future work to characterize the effects of other e-cig product-specific factors such as power levels, heating temperature, solvent mix, and resultant levels of free radicals and aldehydes formed in the aerosol.

With regard to mechanism of VED onset and oxidant stress, the current studies focused on eNOS and NADPH oxidase as sources of vascular ROS. Indeed as discussed earlier, there are a variety of other important pathways of ROS generation that could also contribute to e-cig-induced VED and disease. In the future, it will be important to study these other processes of oxidative stress and free radical production and their role in e-cig-induced oxidant stress, VED, and CVD onset. The role of dysfunctional mitochondria, where ROS production from electron transport chain leak has been previously implicated in many disease processes ranging from ischemia/reperfusion injury to VED (80, 96), will be important to study. In addition, the role of aldehyde oxidase, which can metabolize not only a range of aldehydes such as those formed in the e-cig aerosol but also nicotine metabolites to form ROS, requires dedicated investigation. It will also be important to further characterize the processes that contribute to the loss of NO bioavailability and how e-cig exposure alters vascular and smooth muscle NO metabolism. In addition, there is a need to characterize alterations that occur in the critical antioxidative enzymes and overall redox metabolism.

Conclusion

We observe that chronic ECV exposure induces VED by triggering a vicious cycle of ROS generation, NO depletion, with NADPH oxidase activation and eNOS uncoupling secondary to oxidative BH_4 depletion. Superoxide scavenges NO with peroxynitrite formation that nitrates proteins and can further deplete BH_4. Decreased levels of eNOS are seen, likely due to this process of oxidative modification and degradation. With higher aerosol nicotine concentrations and longer exposure times, the magnitude of ROS generation is increased, leading to increased VED and cardiovascular disease onset. Even in the absence of nicotine, prolonged ECV exposure elevated ROS generation and triggered VED and disease.

GRANTS

This work is supported by The National Heart, Lung, and Blood Institute and The American Lung Association Grants R01HL135648, R01HL131941, and GR120177 (to J. L. Zweier).

DISCLOSURES

No conflicts of interest, financial or otherwise, are declared by the authors.

AUTHOR CONTRIBUTIONS

M.A.E. and J.L.Z. conceived and designed research; M.S.E., M.G.E., and E.M.M. performed experiments; M.A.E., M.G.E., M.S.E., and E.M.M. analyzed data; M.A.E., S.A.K., M.S.E., M.G.E., E.M.M., and J.L.Z. interpreted results of experiments; M.G.E., E.M.M., and M.S.E. prepared figures; M.A.E., S.A.K., and J.L.Z. drafted manuscript; M.A.E., S.A.K., M.G.E., E.M.M., M.S.E., and J.L.Z. edited and revised manuscript; M.A.E., S.A.K., M.G.E., E.M.M., M.S.E., and J.L.Z. approved final version of manuscript.

REFERENCES

1. **Galley HF**, **Webster NR.** Physiology of the endothelium. *Br J Anaesth* 93: 105–113, 2004. doi:10.1093/bja/aeh163.
2. **Palmer RM**, **Ferrige AG**, **Moncada S.** Nitric oxide release accounts for the biological activity of endothelium-derived relaxing factor. *Nature* 327: 524–526, 1987. doi:10.1038/327524a0.
3. **Moncada S**, **Palmer RMJ**, **Higgs EA.** Nitric oxide: physiology, pathophysiology, and pharmacology. *Pharmacol Rev* 43: 109–142, 1991.
4. **White KA**, **Marletta MA.** Nitric oxide synthase is a cytochrome-P-450 type hemoprotein. *Biochemistry* 31: 6627–6631, 1992. doi:10.1021/bi00144a001.

5. **Zweier JL**, **Ilangovan G.** Regulation of nitric oxide metabolism and vascular tone by cytoglobin. *Antioxid Redox Signal* 32: 1172–1187, 2020. doi:10.1089/ars.2019.7881.
6. **Liu XP**, **El-Mahdy MA**, **Boslett J**, **Varadharaj S**, **Hemann C**, **Abdelghany TM**, **Ismail RS**, **Little SC**, **Zhou D**, **Thuy LTT**, **Kawada N**, **Zweier JL.** Cytoglobin regulates blood pressure and vascular tone through nitric oxide metabolism in the vascular wall. *Nat Commun* 8: 14807, 2017. doi:10.1038/ncomms14807.
7. **Halcox JP**, **Narayanan S**, **Cramer-Joyce L**, **Mincemoyer R**, **Quyyumi AA.** Characterization of endothelium-derived hyperpolarizing factor in the human forearm microcirculation. *Am J Physiol Heart Circ Physiol* 280: H2470–H2477, 2001. doi:10.1152/ajpheart.2001.280.6.H2470.
8. **Vanhoutte PM**, **Shimokawa H**, **Feletou M**, **Tang EH.** Endothelial dysfunction and vascular disease - a 30th anniversary update. *Acta Physiol (Oxf)* 219: 22–96, 2017. doi:10.1111/apha.12646.
9. **Huang PL.** Endothelial nitric oxide synthase and endothelial dysfunction. *Curr Hypertens Rep* 5: 473–480, 2003. doi:10.1007/s11906-003-0055-4.
10. **Schulz E**, **Anter E**, **Keaney JF.** Oxidative stress, antioxidants, and endothelial function. *Curr Med Chem* 11: 1093–1104, 2004. doi:10.2174/0929867043365369.
11. **Incalza MA**, **D'Oria R**, **Natalicchio A**, **Perrini S**, **Laviola L**, **Giorgino F.** Oxidative stress and reactive oxygen species in endothelial dysfunction associated with cardiovascular and metabolic diseases. *Vascul Pharmacol* 100: 1–19, 2018. doi:10.1016/j.vph.2017.05.005.
12. **Radi R**, **Beckman JS**, **Bush KM**, **Freeman BA.** Peroxynitrite oxidation of sulfhydryls. The cytotoxic potential of superoxide and nitric oxide. *J Biol Chem* 266: 4244–4250, 1991.
13. **Biondi R**, **Ambrosio G**, **De Pascali F**, **Tritto I**, **Capodicasa E**, **Druhan LJ**, **Hemann C**, **Zweier JL.** HPLC analysis of tetrahydrobiopterin and its pteridine derivatives using sequential electrochemical and fluorimetric detection: application to tetrahydrobiopterin autoxidation and chemical oxidation. *Arch Biochem Biophys* 520: 7–16, 2012. doi:10.1016/j.abb.2012.01.010.
14. **Dumitrescu C**, **Biondi R**, **Xia Y**, **Cardounel AJ**, **Druhan LJ**, **Ambrosio G**, **Zweier JL.** Myocardial ischemia results in tetrahydrobiopterin (BH4) oxidation with impaired endothelial function ameliorated by BH4. *Proc Natl Acad Sci USA* 104: 15081–15086, 2007. doi:10.1073/pnas.0702986104.
15. **Zafari AM**, **Ushio-Fukai M**, **Akers M**, **Yin Q**, **Shah A**, **Harrison DG**, **Taylor WR**, **Griendling KK.** Role of NADH/NADPH oxidase-derived H_2O_2 in angiotensin II-induced vascular hypertrophy. *Hypertension* 32: 488–495, 1998. doi:10.1161/01.hyp.32.3.488.
16. **Chen CA**, **Wang TY**, **Varadharaj S**, **Reyes LA**, **Hemann C**, **Talukder MA**, **Chen YR**, **Druhan LJ**, **Zweier JL.** S-glutathionylation uncouples eNOS and regulates its cellular and vascular function. *Nature* 468: 1115–1118, 2010. doi:10.1038/nature09599.
17. **Cardounel AJ**, **Zweier JL.** Endogenous methylarginines regulate neuronal nitric-oxide synthase and prevent excitotoxic injury. *J Biol Chem* 277: 33995–34002, 2002. doi:10.1074/jbc.M108983200.
18. **Xia Y**, **Tsai AL**, **Berka V**, **Zweier JL.** Superoxide generation from endothelial nitric-oxide synthase. A Ca^{2+}/calmodulin-dependent and tetrahydrobiopterin regulatory process. *J Biol Chem* 273: 25804–25808, 1998. doi:10.1074/jbc.273.40.25804.
19. **Vermot A**, **Petit-Härtlein I**, **Smith SME**, **Fieschi F.** NADPH Oxidases (NOX): an overview from discovery, molecular mechanisms to physiology and pathology. *Antioxidants(Basel)* 10: 890, 2021. doi:10.3390/antiox10060890.
20. **Zhang JQ**, **Chen CF**, **Li L**, **Zhou HJJ**, **Li FH**, **Zhang HF**, **Yu LY**, **Chen YX**, **Min W.** Endothelial AIP_1 regulates vascular remodeling by suppressing NADPH oxidase-2. *Front Physiol* 9: 396, 2018. doi:10.3389/fphys.2018.00396.
21. **Ma MM**, **Gao M**, **Guo KM**, **Wang M**, **Li XY**, **Zeng XL**, **Sun L**, **Lv XF**, **Du YH**, **Wang GL**, **Zhou JG**, **Guan YY.** TMEM16A contributes to endothelial dysfunction by facilitating Nox_2 NADPH oxidase-derived reactive oxygen species generation in hypertension. *Hypertension* 69: 892–901, 2017. doi:10.1161/HYPERTENSIONAHA.116.08874.
22. **Douglas G**, **Bendall JK**, **Crabtree MJ**, **Tatham AL**, **Carter EE**, **Hale AB**, **Channon KM.** Endothelial-specific Nox2 overexpression increases vascular superoxide and macrophage recruitment in ApoE-/-mice. *Cardiovascular Res* 94: 20–29, 2012. doi:10.1093/cvr/cvs026.
23. **Polosa R.** Electronic cigarette use and harm reversal: emerging evidence in the lung. *Bmc Med* 13: 54, 2015. doi:10.1186/s12916-015-0298-3.
24. **Eltorai AE**, **Choi AR**, **Eltorai AS.** Impact of electronic cigarettes on various organ systems. *Respir Care* 64: 328–336, 2019. doi:10.4187/respcare.06300.
25. **Moheimani RS**, **Bhetraratana M**, **Yin F**, **Peters KM**, **Gornbein J**, **Araujo JA**, **Middlekauff HR.** Increased cardiac sympathetic activity and oxidative stress in habitual electronic cigarette users implications for cardiovascular risk. *JAMA Cardiol* 2: 278–284, 2017. doi:10.1001/jamacardio.2016.5303.
26. **Kondo T**, **Nakano Y**, **Adachi S**, **Murohara T.** Effects of tobacco smoking on cardiovascular disease. *Circ J* 83: 1980–1985, 2019. doi:10.1253/circj.CJ-19-0323.
27. **El-Mahdy MA**, **Abdelghany TM**, **Hemann C**, **Ewees MG**, **Mahgoup EM**, **Eid MS**, **Shalaan MT**, **Alzarie YA**, **Zweier JL.** Chronic cigarette smoke exposure triggers a vicious cycle of leukocyte and endothelial-mediated oxidant stress that results in vascular dysfunction. *Am J Physiol Heart Circ Physiol* 319: H51–H65, 2020. doi:10.1152/ajpheart.00657.2019.
28. **Buchanan ND**, **Grimmer JA**, **Tanwar V**, **Schwieterman N**, **Mohler PJ**, **Wold LE.** Cardiovascular risk of electronic cigarettes: a review of preclinical and clinical studies. *Cardiovasc Res* 116: 40–50, 2020. doi:10.1093/cvr/cvz256.
29. **Middlekauff HR.** Cardiovascular impact of electronic-cigarette use. *Trends Cardiovasc Med* 30: 133–140, 2020. doi:10.1016/j.tcm.2019.04.006.
30. **El-Mahdy MA**, **Mahgoup EM**, **Ewees MG**, **Eid MS**, **Abdelghany TM**, **Zweier JL.** Long-term electronic cigarette exposure induces cardiovascular dysfunction similar to tobacco cigarettes: role of nicotine and exposure duration. *Am J Physiol Heart Circ Physiol* 320: H2112–H2129, 2021. doi:10.1152/ajpheart.00997.2020.
31. **Espinoza-Derout J**, **Hasan KM**, **Shao XM**, **Jordan MC**, **Sims C**, **Lee DL**, **Sinha S**, **Simmons Z**, **Mtume N**, **Liu Y**, **Roos KP**, **Sinha-Hikim AP**, **Friedman TC.** Chronic intermittent electronic cigarette exposure induces cardiac dysfunction and atherosclerosis in apolipoprotein-E knockout mice. *Am J Physiol Heart Circ Physiol* 317: H445–H459, 2019. doi:10.1152/ajpheart.00738.2018.
32. **Olfert IM**, **DeVallance E**, **Hoskinson H**, **Branyan KW**, **Clayton S**, **Pitzer CR**, **Sullivan DP**, **Breit MJ**, **Wu Z**, **Klinkhachorn P**, **Mandler WK**, **Erdreich BH**, **Ducatman BS**, **Bryner RW**, **Dasgupta P**, **Chantler PD.** Chronic exposure to electronic cigarettes results in impaired cardiovascular function in mice. *J Appl Physiol (1985)* 124: 573–582, 2018. doi:10.1152/japplphysiol.00713.2017.
33. **Tsai M**, **Byun MK**, **Shin J**, **Crotty Alexander LE.** Effects of e-cigarettes and vaping devices on cardiac and pulmonary physiology. *J Physiol* 598: 5039–5062, 2020. doi:10.1113/JP279754.
34. **Zweier JL**, **Shalaan MT**, **Samouilov A**, **Saleh IG**, **El-Mahdy MA.** Whole body electronic cigarette exposure system for efficient evaluation of diverse inhalation conditions and products. *Inhal Toxicol* 32: 477–486, 2020. doi:10.1080/08958378.2020.1850935.
35. **Talukder MH**, **Morrison RR**, **Mustafa SJ.** Comparison of the vascular effects of adenosine in isolated mouse heart and aorta. *Am J Physiol Heart Circ Physiol* 282: H49–H57, 2002. doi:10.1152/ajpheart.2002.282.1.H49.
36. **Talukder MA**, **Johnson WM**, **Varadharaj S**, **Lian J**, **Kearns PN**, **El-Mahdy MA**, **Liu X**, **Zweier JL.** Chronic cigarette smoking causes hypertension, increased oxidative stress, impaired NO bioavailability, endothelial dysfunction, and cardiac remodeling in mice. *Am J Physiol Heart Circ Physiol* 300: H388–H396, 2011. doi:10.1152/ajpheart.00868.2010.
37. **Gao S**, **Ho D**, **Vatner DE**, **Vatner SF.** Echocardiography in mice. *Curr Protoc Mouse Biol* 1: 71–83, 2011. doi:10.1002/9780470942390.mo100130.
38. **Paulo LL**, **Cruz JC**, **Zhuge Z**, **Carvalho-Galvão A**, **Brandão MCR**, **Diniz TF**, **Haworth SM**, **Athayde-Filho PF**, **Lemos VS**, **Lundberg JO**, **Montenegro MF**, **Braga VA**, **Carlström M.** The novel organic mononitrate NDHP attenuates hypertension and endothelial dysfunction in hypertensive rats. *Redox Biol* 15: 182–191, 2018. doi:10.1016/j.redox.2017.12.004.
39. **Taddei S**, **Virdis A**, **Mattei P**, **Ghiadoni L**, **Sudano I**, **Salvetti A.** Defective L-arginine-nitric oxide pathway in offspring of essential hypertensive patients. *Circulation* 94: 1298–1303, 1996. doi:10.1161/01.CIR.94.6.1298.

40. **Chen CA**, **Druhan LJ**, **Varadharaj S**, **Chen YR**, **Zweier JL.** Phosphorylation of endothelial nitric-oxide synthase regulates superoxide generation from the enzyme. *J Biol Chem* 283: 27038–27047, 2008. doi:10.1074/jbc.M802269200.
41. **Fulton D**, **Gratton JP**, **McCabe TJ**, **Fontana J**, **Fujio Y**, **Walsh K**, **Franke TF**, **Papapetropoulos A**, **Sessa WC.** Regulation of endothelium-derived nitric oxide production by the protein kinase Akt. *Nature* 399: 597–601, 1999. [Erratum in *Nature* 400: 792, 1999]. doi:10.1038/21218.
42. **De Pascali F**, **Hemann C**, **Samons K**, **Chen CA**, **Zweier JL.** Hypoxia and reoxygenation induce endothelial nitric oxide synthase uncoupling in endothelial cells through tetrahydrobiopterin depletion and S-glutathionylation. *Biochemistry* 53: 3679–3688, 2014. doi:10.1021/bi500076r.
43. **Zweier JL**, **Chen CA**, **Druhan LJ.** S-glutathionylation reshapes our understanding of endothelial nitric oxide synthase uncoupling and nitric oxide/reactive oxygen species-mediated signaling. *Antioxid Redox Signal* 14: 1769–1775, 2011. doi:10.1089/ars.2011.3904.
44. **Förstermann U**, **Münzel T.** Endothelial nitric oxide synthase in vascular disease: from marvel to menace. *Circulation* 113: 1708–1714, 2006. doi:10.1161/CIRCULATIONAHA.105.602532.
45. **Marsot A**, **Simon N.** Nicotine and cotinine levels with electronic cigarette: a review. *Int J Toxicol* 35: 179–185, 2016. doi:10.1177/1091581815618935.
46. **Singh T**, **Arrazola RA**, **Corey CG**, **Husten CG**, **Neff LJ**, **Homa DM**, **King BA.** Tobacco use among middle and high school students–united states, 2011-2015. *MMWR Morb Mortal Wkly Rep* 65: 361–367, 2016. doi:10.15585/mmwr.mm6514a1.
47. **Nutt DJ**, **Phillips LD**, **Balfour D**, **Curran HV**, **Dockrell M**, **Foulds J**, **Fagerstrom K**, **Letlape K**, **Milton A**, **Polosa R**, **Ramsey J**, **Sweanor D.** Estimating the harms of nicotine-containing products using the MCDA approach. *Eur Addict Res* 20: 218–225, 2014. doi:10.1159/000360220.
48. **Polosa R**, **Cibella F**, **Caponnetto P**, **Maglia M**, **Prosperini U**, **Russo C**, **Tashkin D.** Health impact of E-cigarettes: a prospective 3.5-year study of regular daily users who have never smoked. *Sci Rep* 7: 13825, 2017. doi:10.1038/s41598-017-14043-2.
49. **Wang P**, **Zweier JL.** Measurement of nitric oxide and peroxynitrite generation in the postischemic heart. Evidence for peroxynitrite-mediated reperfusion injury. *J Biol Chem* 271: 29223–29230, 1996. doi:10.1074/jbc.271.46.29223.
50. **Walsh T**, **Donnelly T**, **Lyons D.** Impaired endothelial nitric oxide bioavailability: a common link between aging, hypertension, and atherogenesis? *J Am Geriatr Soc* 57: 140–145, 2009. doi:10.1111/j.1532-5415.2008.02051.x.
51. **Förstermann U**, **Xia N**, **Li HG.** Roles of vascular oxidative stress and nitric oxide in the pathogenesis of atherosclerosis. *Circ Res* 120: 713–735, 2017. doi:10.1161/CIRCRESAHA.116.309326.
52. **Beckman JS**, **Koppenol WH.** Nitric oxide, superoxide, and peroxynitrite: the good, the bad, and ugly. *Am J Physiol Cell Physiol* 271: C1424–C1437, 1996. doi:10.1152/ajpcell.1996.271.5.C1424.
53. **Beckman JS.** Oxidative damage and tyrosine nitration from peroxynitrite. *Chem Res Toxicol* 9: 836–844, 1996. doi:10.1021/tx9501445.
54. **Thomson L.** 3-nitrotyrosine modified proteins in atherosclerosis. *Dis Markers* 2015: 708282, 2015. doi:10.1155/2015/708282.
55. **Szumska M**, **Wielkoszyński T**, **Tyrpień K.** [3-nitrotyrosine determination as nitrosative stress marker and health attitudes of medical students considering exposure to environmental tobacco smoke]. *Przegl Lek* 69: 798–802, 2012.
56. **Jin H**, **Webb-Robertson BJ**, **Peterson ES**, **Tan R**, **Bigelow DJ**, **Scholand MB**, **Hoidal JR**, **Pounds JG**, **Zangar RC.** Smoking, COPD, and 3-nitrotyrosine levels of plasma proteins. *Environ Health Perspect* 119: 1314–1320, 2011. doi:10.1289/ehp.1103745.
57. **Chen W**, **Druhan LJ**, **Chen CA**, **Hemann C**, **Chen YR**, **Berka V**, **Tsai AL**, **Zweier JL.** Peroxynitrite induces destruction of the tetrahydrobiopterin and heme in endothelial nitric oxide synthase: transition from reversible to irreversible enzyme inhibition. *Biochemistry* 49: 3129–3137, 2010. doi:10.1021/bi9016632.
58. **Abdelghany TM**, **Ismail RS**, **Mansoor FA**, **Zweier JR**, **Lowe F**, **Zweier JL.** Cigarette smoke constituents cause endothelial nitric oxide synthase dysfunction and uncoupling due to depletion of tetrahydrobiopterin with degradation of GTP cyclohydrolase. *Nitric Oxide* 76: 113–121, 2018. doi:10.1016/j.niox.2018.02.009.
59. **McCabe TJ**, **Fulton D**, **Roman LJ**, **Sessa WC.** Enhanced electron flux and reduced calmodulin dissociation may explain "calcium-independent" eNOS activation by phosphorylation. *J Biol Chem* 275: 6123–6128, 2000. doi:10.1074/jbc.275.9.6123.
60. **Dimmeler S**, **Fleming I**, **Fisslthaler B**, **Hermann C**, **Busse R**, **Zeiher AM.** Activation of nitric oxide synthase in endothelial cells by Akt-dependent phosphorylation. *Nature* 399: 601–605, 1999. doi:10.1038/21224.
61. **Iaccarino G**, **Ciccarelli M**, **Sorriento D**, **Cipolletta E**, **Cerullo V**, **Iovino GL**, **Paudice A**, **Elia A**, **Santulli G**, **Campanile A**, **Arcucci O**, **Pastore L**, **Salvatore F**, **Condorelli G**, **Trimarco B.** AKT participates in endothelial dysfunction in hypertension. *Circulation* 109: 2587–2593, 2004. doi:10.1161/01.CIR.0000129768.35536.FA.
62. **Talih S**, **Balhas Z**, **Salman R**, **Karaoghlanian N**, **Shihadeh A.** "Direct dripping": a high-temperature, high-formaldehyde emission electronic cigarette use method. *Nicotine Tob Res* 18: 453–459, 2016. doi:10.1093/ntr/ntv080.
63. **Lerner CA**, **Sundar IK**, **Yao H**, **Gerloff J**, **Ossip DJ**, **McIntosh S**, **Robinson R**, **Rahman I.** Vapors produced by electronic cigarettes and e-juices with flavorings induce toxicity, oxidative stress, and inflammatory response in lung epithelial cells and in mouse lung. *PLoS One* 10: e0116732, 2015. doi:10.1371/journal.pone.0116732.
64. **Carnevale R**, **Sciarretta S**, **Violi F**, **Nocella C**, **Loffredo L**, **Perri L**, **Peruzzi M**, **Marullo AGM**, **De Falco E**, **Chimenti I**, **Valenti V**, **Biondi-Zoccai G**, **Frati G.** Acute impact of tobacco vs electronic cigarette smoking on oxidative stress and vascular function. *Chest* 150: 606–612, 2016. doi:10.1016/j.chest.2016.04.012.
65. **Matsuno K**, **Yamada H**, **Iwata K**, **Jin D**, **Katsuyama M**, **Matsuki M**, **Takai S**, **Yamanishi K**, **Miyazaki M**, **Matsubara H**, **Yabe-Nishimura C.** Nox1 is involved in angiotensin II-mediated hypertension - A study in Nox1-deficient mice. *Circulation* 112: 2677–2685, 2005. doi:10.1161/CIRCULATIONAHA.105.573709.
66. **Hink U**, **Li H**, **Mollnau H**, **Oelze M**, **Matheis E**, **Hartmann M**, **Skatchkov M**, **Thaiss F**, **Stahl RA**, **Warnholtz A**, **Meinertz T**, **Griendling K**, **Harrison DG**, **Forstermann U**, **Munzel T.** Mechanisms underlying endothelial dysfunction in diabetes mellitus. *Circ Res* 88: E14–E22, 2001. doi:10.1161/01.res.88.2.e14.
67. **Warnholtz A**, **Nickenig G**, **Schulz E**, **Macharzina R**, **Bräsen JH**, **Skatchkov M**, **Heitzer T**, **Stasch JP**, **Griendling KK**, **Harrison DG**, **Böhm M**, **Meinertz T**, **Münzel T.** Increased NADH-oxidase-mediated superoxide production in the early stages of atherosclerosis: evidence for involvement of the renin-angiotensin system. *Circulation* 99: 2027–2033, 1999. doi:10.1161/01.cir.99.15.2027.
68. **Lassegue B**, **Clempus RE.** Vascular NAD(P)H oxidases: specific features, expression, and regulation. *Am J Physiol Regul Integr Comp Physiol* 285: R277–R297, 2003. doi:10.1152/ajpregu.00758.2002.
69. **Touyz RM**, **Schiffrin EL.** Increased generation of superoxide by angiotensin II in smooth muscle cells from resistance arteries of hypertensive patients: role of phospholipase D-dependent NAD(P)H oxidase-sensitive pathways. *J Hypertens* 19: 1245–1254, 2001. doi:10.1097/00004872-200107000-00009.
70. **Kuntic M**, **Oelze M**, **Steven S**, **Kröller-Schön S**, **Stamm P**, **Kalinovic S**, **Frenis K**, **Vujacic-Mirski K**, **Jimenez MTB**, **Kvandova M**, **Filippou K**, **Al Zuabi A**, **Brückl V**, **Hahad O**, **Daub S**, **Varveri F**, **Gori T**, **Huesmann R**, **Hoffmann T**, **Schmidt FP**, **Keaney JF**, **Daiber A**, **Münzel T.** Short-term e-cigarette vapour exposure causes vascular oxidative stress and dysfunction: evidence for a close connection to brain damage and a key role of the phagocytic NADPH oxidase (NOX-2). *Eur Heart J* 41: 2472–2483, 2020. doi:10.1093/eurheartj/ehz772.
71. **Alkaitis MS**, **Crabtree MJ.** Recoupling the cardiac nitric oxide synthases: tetrahydrobiopterin synthesis and recycling. *Curr Heart Fail Rep* 9: 200–210, 2012. doi:10.1007/s11897-012-0097-5.
72. **Hattori Y**, **Hattori S**, **Wang X**, **Satoh H**, **Nakanishi N**, **Kasai K.** Oral administration of tetrahydrobiopterin slows the progression of atherosclerosis in apolipoprotein E-knockout mice. *Arterioscler Thromb Vasc Biol* 27: 865–870, 2007. doi:10.1161/01.ATV.0000258946.55438.0e.
73. **Landmesser U**, **Dikalov S**, **Price SR**, **McCann L**, **Fukai T**, **Holland SM**, **Mitch WE**, **Harrison DG.** Oxidation of tetrahydrobiopterin leads to uncoupling of endothelial cell nitric oxide synthase in hypertension. *J Clin Invest* 111: 1201–1209, 2003. doi:10.1172/JCI14172.
74. **Alp NJ**, **Mussa S**, **Khoo J**, **Cai S**, **Guzik T**, **Jefferson A**, **Goh N**, **Rockett KA**, **Channon KM.** Tetrahydrobiopterin-dependent

preservation of nitric oxide-mediated endothelial function in diabetes by targeted transgenic GTP-cyclohydrolase I overexpression. *J Clin Invest* 112: 725–735, 2003. doi:10.1172/JCI17786.

75. **Vásquez-Vivar J**, **Whitsett J**, **Martásek P**, **Hogg N**, **Kalyanaraman B.** Reaction of tetrahydrobiopterin with superoxide: EPR-kinetic analysis and characterization of the pteridine radical. *Free Radic Biol Med* 31: 975–985, 2001. doi:10.1016/s0891-5849(01)00680-3.
76. **Amici M**, **Sagratini D**, **Pettinari A**, **Pucciarelli S**, **Angeletti M**, **Eleuteri AM.** 20S proteasome mediated degradation of DHFR: implications in neurodegenerative disorders. *Arch Biochem Biophys* 422: 168–174, 2004. doi:10.1016/j.abb.2003.12.014.
77. **Kim M**, **Han C-H**, **Lee M-Y.** NADPH oxidase and the cardiovascular toxicity associated with smoking. *Toxicol Res* 30: 149–157, 2014. doi:10.5487/TR.2014.30.3.149.
78. **Zweier JL**, **Talukder MA.** The role of oxidants and free radicals in reperfusion injury. *Cardiovasc Res* 70: 181–190, 2006. doi:10.1016/j.cardiores.2006.02.025.
79. **Dikalov S.** Cross talk between mitochondria and NADPH oxidases. *Free Radic Biol Med* 51: 1289–1301, 2011. doi:10.1016/j.freeradbiomed.2011.06.033.
80. **Zweier JL**, **Flaherty JT**, **Weisfeldt ML.** Direct measurement of free radical generation following reperfusion of ischemic myocardium. *Proc Natl Acad Sci USA* 84: 1404–1407, 1987. doi:10.1073/pnas.84.5.1404.
81. **Zorov DB**, **Filburn CR**, **Klotz LO**, **Zweier JL**, **Sollott SJ.** Reactive oxygen species (ROS)-induced ROS release: a new phenomenon accompanying induction of the mitochondrial permeability transition in cardiac myocytes. *J Exp Med* 192: 1001–1014, 2000. doi:10.1084/jem.192.7.1001.
82. **Konior A**, **Schramm A**, **Czesnikiewicz-Guzik M**, **Guzik TJ.** NADPH oxidases in vascular pathology. *Antioxid Redox Signal* 20: 2794–2814, 2014. doi:10.1089/ars.2013.5607.
83. **Buvelot H**, **Jaquet V**, **Krause KH.** Mammalian NADPH oxidases. *Methods in molecular biology (Clifton, NJ)* 1982: 17–36, 2019. doi:10.1007/978-1-4939-9424-3_2.
84. **Zainalabidin S**, **Budin SB**, **Ramalingam A**, **Lim YC.** Aortic remodelling in chronic nicotine-administered rat. *Korean J Physiol Pharmacol* 18: 411–418, 2014. doi:10.4196/kjpp.2014.18.5.411.
85. **Si LY**, **Kamisah Y**, **Ramalingam A**, **Lim YC**, **Budin SB**, **Zainalabidin S.** Roselle supplementation prevents nicotine-induced vascular endothelial dysfunction and remodelling in rats. *Appl Physiol Nutr Metab* 42: 765–772, 2017. doi:10.1139/apnm-2016-0506.
86. **Hukkanen J**, **Jacob P 3rd**, **Benowitz NL.** Metabolism and disposition kinetics of nicotine. *Pharmacol Rev* 57: 79–115, 2005. doi:10.1124/pr.57.1.3.
87. **Goldstein DS**, **Kopin IJ**, **Sharabi Y.** Catecholamine autotoxicity. Implications for pharmacology and therapeutics of Parkinson disease and related disorders. *Pharmacol Ther* 144: 268–282, 2014. doi:10.1016/j.pharmthera.2014.06.006.
88. **Moheimani RS**, **Bhetraratana M**, **Peters KM**, **Yang BK**, **Yin F**, **Gornbein J**, **Araujo JA**, **Middlekauff HR.** Sympathomimetic effects of acute e-cigarette use: role of nicotine and non-nicotine constituents. *J Am Heart Assoc* 6: e006579, 2017. doi:10.1161/JAHA.117.006579.
89. **Chatterjee S**, **Tao JQ**, **Johncola A**, **Guo W**, **Caporale A**, **Langham MC**, **Wehrli FW.** Acute exposure to e-cigarettes causes inflammation and pulmonary endothelial oxidative stress in nonsmoking, healthy young subjects. *Am J Physiol Lung Cell Mol Physiol* 317: L155–L166, 2019. doi:10.1152/ajplung.00110.2019.
90. **Chaumont M**, **de Becker B**, **Zaher W**, **Culié A**, **Deprez G**, **Mélot C**, **Reyé F**, **Van Antwerpen P**, **Delporte C**, **Debbas N**, **Boudjeltia KZ**, **van de Borne P.** Differential effects of e-cigarette on microvascular endothelial function, arterial stiffness and oxidative stress: a randomized crossover trial. *Sci Rep* 8: 10378–10378, 2018. doi:10.1038/s41598-018-28723-0.
91. **Benowitz NL**, **Fraiman JB.** Cardiovascular effects of electronic cigarettes. *Nat Rev Cardiol* 14: 447–456, 2017. doi:10.1038/nrcardio.2017.36.
92. **Seals DR**, **Jablonski KL**, **Donato AJ.** Aging and vascular endothelial function in humans. *Clin Sci (Lond)* 120: 357–375, 2011. doi:10.1042/CS20100476.
93. **Yamamoto K**, **Takeshita K**, **Kojima T**, **Takamatsu J**, **Saito H.** Aging and plasminogen activator inhibitor-1 (PAI-1) regulation: implication in the pathogenesis of thrombotic disorders in the elderly. *Cardiovasc Res* 66: 276–285, 2005. doi:10.1016/j.cardiores.2004.11.013.
94. **Brandes RP**, **Fleming I**, **Busse R.** Endothelial aging. *Cardiovasc Res* 66: 286–294, 2005. doi:10.1016/j.cardiores.2004.12.027.
95. **Blackwell KA**, **Sorenson JP**, **Richardson DM**, **Smith LA**, **Suda O**, **Nath K**, **Katusic ZS.** Mechanisms of aging-induced impairment of endothelium-dependent relaxation: role of tetrahydrobiopterin. *Am J Physiol Heart Circ Physiol* 287: H2448–H2453, 2004. doi:10.1152/ajpheart.00248.2004.
96. **Schulz E**, **Gori T**, **Münzel T.** Oxidative stress and endothelial dysfunction in hypertension. *Hypertens Res* 34: 665–673, 2011. doi:10.1038/hr.2011.39.